T-943

FREQUENCY-RESPONSE CHARACTERISTICS OF FIXED-BED ADSORPTION SYSTEMS OF PROPYLENE-PROPANE OVER SILICA GEL

by

Mark Plummer

T-943

A Thesis submitted to the Faculty and the Board of Trustees of the Colorado School of Mines in partial fulfillment of the requirements for the degree of Master of Science in Petroleum Refining engineering.

Signed: Mark A. Plummer
Student

Golden, Colorado
Date: February, 1963

Approved: Lyman W Morgan
Thesis Advisor

James H Gary
Head of Department

Golden, Colorado
Date: Feb. 21, 1963

ABSTRACT

This thesis is a study of the rate parameters describing the rate-controlling mechanisms for adiabatic, fixed-bed adsorption systems of propylene-propane over silica gel.

Frequency-response analyses were made by passing binary mixtures of the above gases, the compositions of which were varied sinusoidally, through beds of silica gel. Combined heat effects and mass transfer effects, rate-controlling mechanisms, caused changes in the amplitudes of these composition waves and shifts in their phases with respect to the input waves. The amplitude and phase changes between the inputs and outputs of the systems corresponding to each frequency of the input sine waves were tabulated in the form of Bode plots.

It has been proposed that differential fixed-bed adsorption systems can be compared to electrical notch-filters; however, experimental data revealed several

resonant frequencies for each adsorption system instead of just one as predicted by filter theory. The first resonant frequency of each bed was associated with the bed functioning like a differential adsorption system. A relationship was then developed between the ratio of the output-to-input composition amplitude for the first resonant frequency and the ratio of R/R_i. The term R represents the resistance to mass diffusion between the bulk phase and the solid phase, and the term R_i represents the resistance to mass diffusion in the interstitial spaces. No explanation of the resonances other than the first is offered.

Experimental apparatus and procedures have been successfully developed with which the frequency response characteristics of adsorption systems can be obtained. Extensive experimentation with this method is recommended to find more fundamental correlations between frequency response results and the rate parameters of adsorption.

CONTENTS

FIGURES

PHOTOGRAPHS

TABLES

ACKNOWLEDGMENTS

The author wishes to express his sincere appreciation for the guidance of Dr. Lyman W. Morgan in directing this investigation. Appreciation is extended to Dr. John T. Williams and Mr. Raymond R. Gutzman for serving as thesis committee members.

Acknowledgment is made of the fellowships provided by the Phillips Petroleum Company and by the Colorado School of Mines.

Appreciation is offered to my wife, Jan, for her help in preparing the final manuscript.

INTRODUCTION

The development of processes such as alkylation to produce high-octane gasoline and polymerization to produce polypropylene has created a demand for large quantities of propylene. Because propylene-propane mixtures are by-products usually available from petroleum refining operations, it becomes economically attractive, therefore, to develop a process that can fractionate propylene from these mixtures.

Fractional distillation, industrially the most common method of fractionating petroleum hydrocarbon mixtures, requires a minimum of 50 equilibrium stages to separate a propylene-propane mixture into an overhead product containing 99 percent propylene and a bottoms product containing 99 percent propane. The preceding was calculated using the Fenske method and a relative volatility of 1.2 (Maxwell, 1957, p. 64). Previous experimentation (Lewis, Gilliland, Chertow, and Cadogan, 1950, p. 1320) has shown

the relative volatility for gaseous propylene-propane mixtures in equilibrium with silica gel to vary about 3.1 with propane being the most volatile component. As a consequence, it can be shown (Mantell, 1951, p. 291) that a minimum of 10 equilibrium stages are required to obtain a 99 percent propane product-stream from a 99 percent propylene inlet-stream by adsorbing the propylene on silica gel. Therefore, in terms of equilibrium selective adsorption of propylene on silica gel seems to offer an efficient method of fractionating the above mixtures.

Before the design of an industrial unit can be contemplated, however, not only must equilibrium data be available but also rate data indicating the speed at which the equilibrium is approached. In fixed-bed adsorption systems the mechanisms controlling the equilibrium rate fall under two general classifications. One is the diffusion of mass and heat resulting from concentration and temperature gradients between the bulk phase and the interior of the solid phase. The other is the diffusion of mass and heat in the interstitial spaces resulting from concentration and temperature gradients along the axes of the confining vessel.

The purpose of this thesis is to study experimentally the rate parameters describing the above rate-controlling mechanisms for adiabatic, fixed-bed adsorption systems of propylene-propane over silica gel. The method used employs the techniques of frequency-response analysis.

Experimentally, frequency-response analysis consists of subjecting the input of a system to a sinusoidal variation of fixed amplitude and recording on two adjoining charts this input along with the resulting output of the system. As the input wave passes through the system, the controlling rate mechanisms may cause a change in its amplitude and a shift in its phase. If the rate mechanisms can be described by linear differential equations with constant coefficients, the wave at any point in the system will be sinusoidal and will exhibit the same frequency as that of the input wave. The results of a frequency-response analysis are the tabulations of the amplitude and phase change pairs between the input and output of the system, one pair for each frequency of the input sine wave. The "Bode Plot" of these data consists of two graphs. One shows the relation between the log of the amplitude ratio, $|KG|$, ratio of output to input amplitude, and the log of the frequency. The other shows the relation between the phase shift, $/\underline{KG}$, and the log of the frequency.

The sinusoidally varying input to the system studied in this thesis is the composition of a propylene-propane gas mixture at constant temperature, pressure, and total bulk flow rate. The system is nonlinear, however, for two reasons. First, the total amount of material that can be adsorbed per unit weight of gel will not remain constant as the input composition wave varies through one cycle. This nonlinearity results because the adsorption capacity of silica gel for propylene is approximately 1.5 times greater than that for propane (Lewis, Gilliland, Chertow, and Cadogan, 1950, p. 1324). However, this nonlinearity can be considered negligible if the deviation of the input composition wave is held to within limits of approximately ±4 mole percent propylene around an equal-molar mean composition. Second, the heat of adsorption of propylene on silica gel is approximately twice that for propane (Shimoda, unpublished) thereby resulting in cycling values for the bed temperature, the temperature dependent rate parameters, and the total adsorption capacity of the gel.

A complete mathematical model that would represent this system would be very complex and is beyond the scope of this thesis; however, a comparison is made between this system and an electrical notch-filter. This comparison indicates how the ratio of the resistances to mass diffusion

varies with changes in the particle size of the solid phase and with changes in the bulk flow rate. The above ratio of resistances is defined as the ratio of the resistance to mass diffusion between the bulk phase and the solid phase to the resistance to mass diffusion in the interstitial spaces.

Frequency-response analysis, as a technique for measuring the magnitudes of the chemical and physical rate mechanisms controlling a system, is relatively new to the chemical engineering field. One of the first applications of this technique to mass transfer was made by Rosen and Winsche (1950, p. 1587-1592). They developed the mathematical relationships between the amplitude and phase changes and the rate mechanisms controlling the following systems subjected to isothermal conditions: opposing first-order chemical reactions and the solid diffusion into the interior of homogeneous spheres in a packed bed with and without the effect of an effective film surrounding the spheres.

Deisler and Wilhelm (1953, p. 1219-27) extended the above work mathematically by taking into account axial diffusion in the interstitial spaces of a fixed-bed adsorption system. Experimentally their systems consisted of binary mixtures of H_2-N_2, C_2H_4-N_2, and C_2H_6-N_2 and porous Norton Alundun catalyst supports. The limitations in their

development were that the system was necessarily isothermal and that the relative volatility of the binary gas mixture in equilibrium with the solid phase was necessarily unity.

The application of frequency-response analysis to the phenomenon of radial mixing of a gas in an open tube has been studied by Keyes (1955, p. 305-311). He developed the mathematical relationship between the amplitude attenuation of a composition wave passing through an open tube and the equivalent gas-film thickness at the wall of the tube. From the thickness of the gas film he was able to calculate values for the radial diffusivity.

Campbell (1958, p. 102) has shown the frequency-response characteristics of a fluid-flow pulsation-damper by developing the analogies between this system and an electrical notch-filter. It has already been noted that a similar analogy will be used in this thesis.

THEORETICAL CONSIDERATIONS

The theoretical considerations are developed by first discussing the analogies that exist between fixed-bed adsorption systems and electrical notch-filters. Secondarily, the composition amplitude ratio at the first resonance is related to literature correlations for the resistances to mass diffusion.

Analogies Between Fixed-Bed Adsorption Systems and Electrical Notch-Filters

The frequency-response characteristics of fixed-bed adsorption systems resemble those of electrical notch-filters or those of any flow system in which the rate-controlling mechanisms can show resonance in a portion of the system parallel to the main flow. Consider the typical electrical notch-filter of Figure 1. A current balance yields the following equation for the ratio of the output

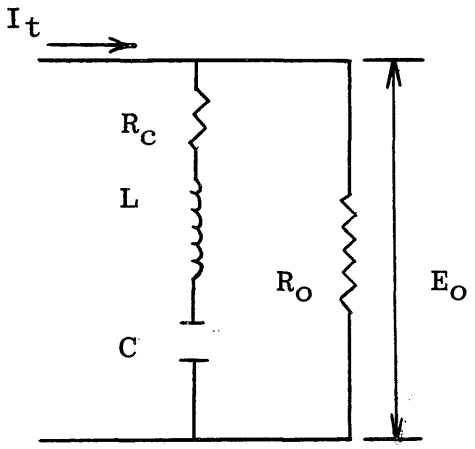

Figure 1: Typical electrical notch-filter

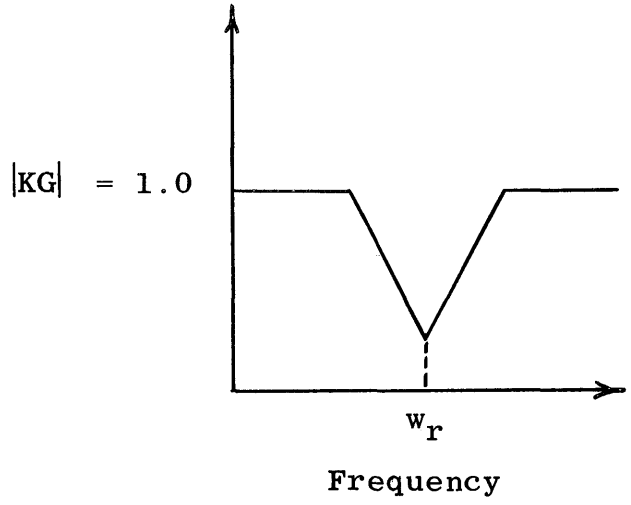

Figure 2: Amplitude ratio vs frequency for a typical notch-filter

voltage, E_o, at any frequency to the voltage, I_tR_o:

$$KG = \frac{E_o}{I_tR_o} = \frac{\frac{R_c}{R_o} + \frac{1}{R_o}\left[jwL + \frac{1}{jwC}\right]}{1 + \frac{R_c}{R_o} + \frac{1}{R_o}\left[jwL + \frac{1}{jwC}\right]} \qquad (1)$$

where w = frequency (radians/sec)

$1/jwC$ = capacitive reactance

jwL = inductive reactance

It can be proved that the amplitude ratio, absolute value of Equation 1, vs. frequency plot for a typical notch-filter will be as shown in Figure 2 if the total current is varied sinusoidally at a constant amplitude over a range of frequencies. The resonant frequency, w_r, is the frequency at which the sum of the capacitive and inductive reactances equals zero.

$$w_r = (1/LC)^{1/2} \qquad (2)$$

The amplitude ratio at the resonant frequency can be related to the two resistances as follows:

$$\frac{R_c}{R_o} = \frac{|KG|_{w_r}}{1 - |KG|_{w_r}} \qquad (3)$$

In a fixed-bed adsorption system, the compositions of the bulk-fluid phase at the outlet and inlet of the bed are analogous to the voltages E_o and I_tR_o, respectively,

in the above notch-filter. The resistance, R, to mass diffusion between the bulk fluid phase and the solid phase is analogous to the resistance R_c. The resistance, R_i, to mass diffusion in the interstitial spaces is analogous to the resistance, R_o.

Capacitance is defined electrically as the ratio of the time rate of change of the amount of charge stored, apparent current, to the time rate of change of the potential causing the storage. In a fixed-bed adsorption system, the material being adsorbed is analogous to the storage of charge; the concentration of the solid phase is analogous to the potential causing the storage. The amount of the bulk phase surrounding the solid phase also represents storage; however, for the studied beds it equals only 3 percent of the amount adsorbed in the beds. Capacitance, which is a dynamic parameter, should not be confused with the equilibrium adsorption capacity, which is a steady-state parameter.

Inductance is defined as the ratio of a potential to a time rate of change of current. The heat of adsorption in a fixed-bed adsorption system will cause, by changing the temperature of the solid phase, a change in the equilibrium adsorption capacity of the bed. The resulting flow of mass will cause a time rate of change in the mass

flow produced by the concentration gradient between the bulk and the solid phase. Therefore, an inductance effect is inherent in a fixed-bed adsorption system with the bed temperature representing a potential causing a time rate of change in a mass flow.

The analogies between a fixed-bed adsorption system and a simple electrical notch-filter are exact only if the adsorption system is of the differential type: an adsorption system in which every particle is subjected to the exact same conditions at every instant. If an adsorption system is not of the differential type, it becomes a distributed parameter system, and the analogies between it and an electrical notch-filter, lumped parameter system, will not be exact.

In the experimental data of this thesis, several resonant frequencies instead of just one were revealed on the composition Bode plots. This data would indicate that the adsorption systems used were not of the differential type over the entire frequency range studied. However, it is assumed that the first resonant frequencies can be associated with the beds acting like differential adsorption systems. Two experimental results substantiate this assumption. One is that the variations in the first resonant frequencies for the two beds studied at the two

bulk flow rates were not the same. The other is that the first resonances for the phase shifts occur at the second resonances for the amplitude ratios for all the beds studied. With the above assumption the ratios of R/R_i can be calculated from the experimental data by using Equation 3 and the composition amplitude ratios at the first resonant frequencies. The ratio of R/R_i is the ratio of the resistance to mass diffusion between the bulk fluid phase and the solid phase to the resistance to mass diffusion in the interstitial spaces.

No explanation of the resonances other than the first is offered except to point out their resemblance to standing waves. Thus, it might be that each one relates to a different depth of material penetration into the gel particles or into a different set of harmonic oscillators into which the bed divides.

Relationship Between the Amplitude Ratio at the First Resonance and the Resistances to Mass Diffusion

The total resistance to the diffusion of mass between the bulk phase and the interior of the solid phase is composed of two parts. The first is that offered by an effective film surrounding each particle. The magnitude of this resistance is proportional to the product of a transfer coefficient and the total external surface area

of the particles. The second is that offered by the porous particles, an exact description of which would be very complex. However, if the pores are considered to be homogeneously distributed in the particles, an effective diffusion coefficient, diffusivity, can be used to describe the average conductance of mass within the particles. The diffusion of mass in the interstitial spaces also is usually described using an effective diffusivity. These diffusivities can be related to the resistances to diffusion by comparing the standard flow law with Fick's law.

Flow law: $q = -\triangle c/R$

Fick's law: $q/A = -D(\triangle c/\triangle x)$

where $\triangle c/\triangle x$ is used to approximate dc/dx

q = flow

A = area for diffusion

$\triangle c$ = concentration difference

$\triangle x$ = length of diffusion

R = resistance

D = diffusivity

From these two laws the following can be derived.

$$\text{Resistance} = \frac{\text{length of diffusion}}{(\text{diffusivity})\ (\text{area for diffusion})} \quad (4)$$

Wilke and Hougen (1945, p. 450) have developed the following relationship for the effective film mass-transfer

coefficient for gases flowing over packed beds of granular material:

$$k_g = \frac{1.82}{M} G \left[\frac{DpG}{\mu}\right]^{-0.51} \left[\frac{\mu}{\rho_f D_v}\right]^{-2/3} \quad (5)$$

where $\frac{DpG}{\mu}$ = particle Reynolds number Re_p

$\frac{DpG}{\mu} < 350$

k_g = mass-transfer coefficient (g moles/cm^2-sec)

D_p = average particle diameter (cm)

D_v = molecular diffusivity (cm^2/sec)

G = mass velocity (gm/cm^2-sec)

M = mean molecular weight (gm/gmole)

ρ_f = mean gas density (gm/cc)

μ = mean gas viscosity (gm/cm-sec)

The total external surface area for a packed bed can be calculated using:

$$A = \frac{6W}{D_p \rho_s} \quad (6)$$

where A = external surface area (cm^2)

W = total weight of bed (gm)

ρ_s = particle density (gm/cc)

The following equation can be derived, p. 79, using equations 5 and 6:

$$R_f(\text{sec/cc}) = \frac{1}{k_g A} = 0.0083 \frac{D_p^{1.51}}{G^{0.49}} \qquad (7)$$

Wheeler (1951, p. 272) has substantiated that the mass diffusional mechanisms in the pores of typical silica gels are of the Knudsen type. Therefore, the resistance to mass diffusion in the solid phase can be related to the particle diameter as follows:

$$R_s = \frac{r\lambda}{D_k A'} \qquad (8)$$

where D_k = Knudsen diffusivity (cm^2/sec)

r = particle radius (cm)

A' = average internal geometric area of the particles, (1/2)A

λ = labyrinth factor

The purpose of the labyrinth factor is to account for the following complications exhibited by porous material such as silica gel. First, the actual diffusion length between two points is usually greater than the straight line distance between the two points. Second, the pore radius along any diffusion path will not be constant; third, the actual area for diffusion is always less than the geometric area. The magnitude of this labyrinth factor will be greater than unity.

The following equation can be derived, p. 80, to describe the relationship between the resistance to mass diffusion in the solid phase and the particle diameter:

$$R_s \text{ (sec/cc)} = 22 \lambda D_p^2 \qquad (9)$$

The sum of Equations 7 and 9 represents the total resistance, R, to mass diffusion between the bulk phase and the solid phase. The following table shows the calculated values for each of the above resistances at the mass velocities and the particle sizes studied. It can be concluded that the resistance of the solid phase is the controlling resistance in each case.

G	D_p	R_f	R_s	R
gm/cm^2-sec	cm	sec/cc	sec/cc	sec/cc
4.60×10^{-3}	0.0975	0.0035	0.21λ	0.21λ
4.60×10^{-3}	0.184	0.0091	0.75λ	0.75λ
4.60×10^{-3}	0.278	0.017	1.7λ	1.7λ
4.60×10^{-3}	0.390	0.028	3.3λ	3.3λ
4.60×10^{-3}	0.585	0.052	7.5λ	7.5λ
9.20×10^{-3}	0.0975	0.0025	0.21λ	0.21λ
9.20×10^{-3}	0.585	0.037	7.5λ	7.5λ

Table 1: Resistance to mass diffusion between the bulk phase and the solid phase

A bulk-phase concentration gradient will exist in the direction of flow because as one component of the binary mixture is being adsorbed, the other is being deadsorbed. The effective diffusivity describing the resulting diffusion of mass has been correlated by Fahien and Smith (1955, p. 35).

$$\frac{D_p G}{\rho_f D_i} = C + 19.4C\ (D_p/D_t)^2 \qquad (10)$$

where D_i = effective mass diffusivity in the interstitial spaces

D_t = diameter of vessel

C = a constant equal to 9 for $30 < D_p G/\mu < 700$.

a variable less than 9 for $D_p G/\mu < 30$.

The corresponding interstitial resistance to diffusion, R_i, is difficult to define because the length of diffusion is unknown and because both the length of and area for diffusion will vary with particle size resulting from variations in the void fraction. However, in the development, p. 80, of the following equation, an average value of 0.4 was assumed for the void fraction and thereby limited the area for diffusion to one value.

$$R_i\ (\text{sec/cc}) = 0.001\ LC \left[\frac{1.22 + 6.02\ D_p^2}{D_p G} \right] \qquad (11)$$

where L = length of diffusion

Table 2 shows the calculated values for the interstitial resistance and the ratio of R/R_i at the mass velocities and particle sizes studied.

G	D_p	R_i	R/R_i
gm/cm^2-sec	cm	sec/cc	
4.60×10^{-3}	0.0975	---	---
4.60×10^{-3}	0.184	8.4L	0.089 λ/L
4.60×10^{-3}	0.278	9.2L	0.18 λ/L
4.60×10^{-3}	0.390	9.6L	0.34 λ/L
4.60×10^{-3}	0.585	11L	0.68 λ/L
9.20×10^{-3}	0.0975	8.5L	0.026 λ/L
9.20×10^{-3}	0.585	5.5L	1.4 λ/L

Table 2: Interstitial resistances and R/R_i ratios

Experimental values of the ratio R/R_i were obtained by using Equation 3 and the composition amplitude ratios at the first resonant frequencies. These experimental values along with the calculated values of R/R_i of Table 2 are plotted vs particle diameter for comparison.

INSTRUMENTATION AND EQUIPMENT

Instrumentation and equipment used in this thesis can best be described under the following sub-headings: overall flow system, composition-wave generator, composition- and temperature-measurement systems, silica-gel beds.

Overall Flow System

The overall flow system is presented schematically in Figure 3 and pictorially by the photographs in Appendix II.

Streams of gaseous propylene and propane (99 mole percent minimum purity) pass from their cylinders through a glycol constant-temperature bath and then through Moore, model 63BD-L, flow controllers. The purpose of these controllers is to keep the propylene and propane flows to the composition-wave generator constant and equal. After passing the composition-wave generator, the two streams are mixed just prior to the input thermistor cell. Part of the mixed stream, the composition of which is now varying

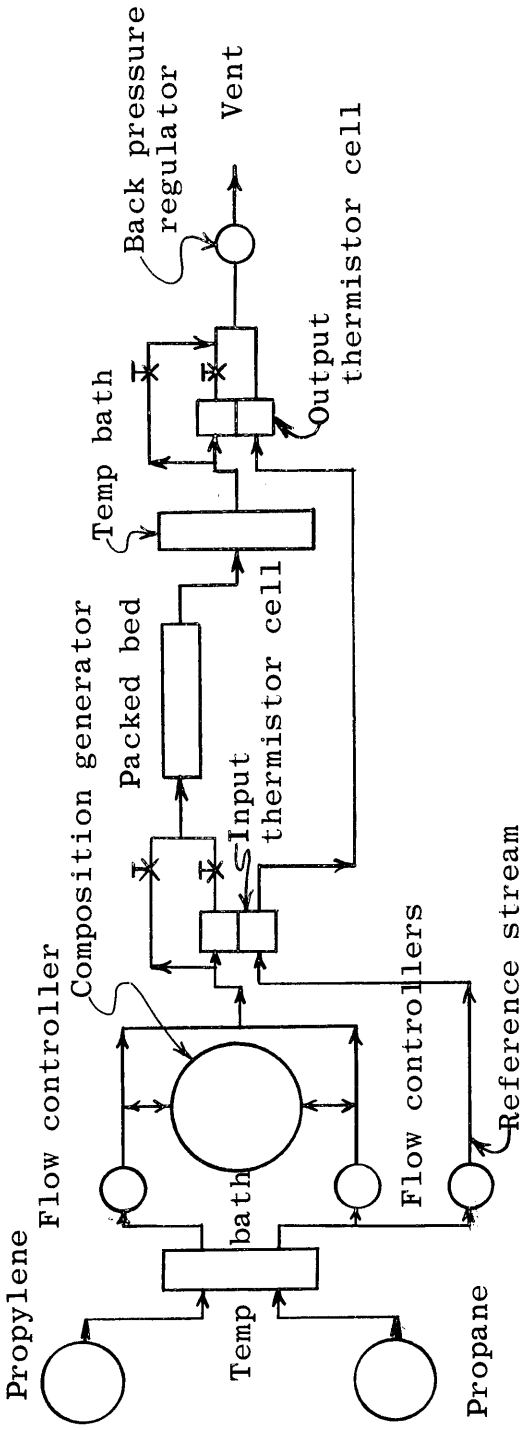

Figure 3: Overall flow system

sinusoidally, passes through the input thermistor cell for composition measurement. The rest of the mixed stream must be bypassed around the thermistor cell since flows larger than 1 cc/sec through the thermistor cell will produce turbulent flow noise that will complicate the composition signal. The recombined stream then enters a packed bed of silica gel where combined heat effects and mass transfer effects may cause a change in the amplitude of the composition wave and a shift in its phase with respect to the input wave. After the mixed stream leaves the packed bed, it re-enters the glycol constant-temperature bath to remove any temperature fluctuations before it enters the output thermistor cell for final composition analysis. After leaving the output thermistor cell, the mixed stream is combined with a pure propane reference stream that has been used as a standard in both composition measurements. The combined stream flows to vent through a Moore, model 43R, absolute-pressure relief valve that holds a constant absolute back-pressure on the entire system.

All measurements of flow were made by timing the rise of a soap bubble in a calibrated burette. The small flows of 1 to 20 cc/sec used in this thesis can be determined accurately to 2 significant figures by this method. The bed pressure was determined by attaching a water manometer to the outlet of the silica gel bed.

Composition-Wave Generator

For applying the technique of frequency-response analysis to the system under study in this thesis, a device was designed that would sinusoidally vary the composition of a gas stream without affecting its total flow rate or its total pressure. Sinusoidal variations of flow have been produced by the sinusoidal displacement of a piston in a feed line (Pauls, Olt, Romano, and Stanton, 1960, p. 48). As depicted in Figure 4, if two cylinders of equal dimensions are connected with a common piston rod and the streams blended some time after leaving their respective cylinders, the flow variations of one will cancel the variations of the other. This leaves only the composition of the blended stream to vary sinusoidally.

This type of device is not limited, however, to sinusoidal variations of composition. The composition of the blended gas stream will always be proportional to the derivative of the displacement applied to the common piston rod.

Figure 5 schematically presents the equipment used in this thesis to obtain the sinusoidal variation needed. An electrical sinusoidal signal was generated by a Donner analog computor and converted to a pneumatic sinusoidal signal by a Fisher, model 545, electro-pneumatic transducer.

$x = x_o + L\sin(wt)$

x = Displacement

L = Center to peak stroke

w = Frequency

t = time

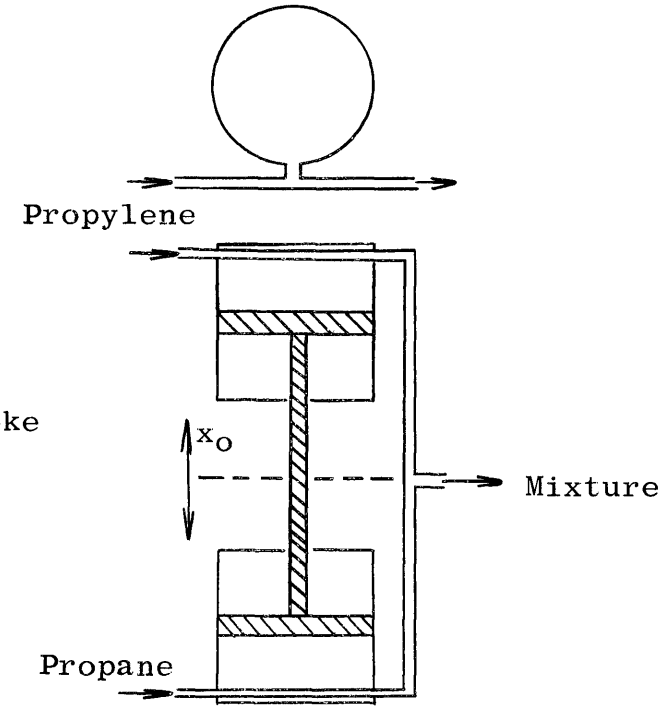

Figure 4: Composition-wave generator

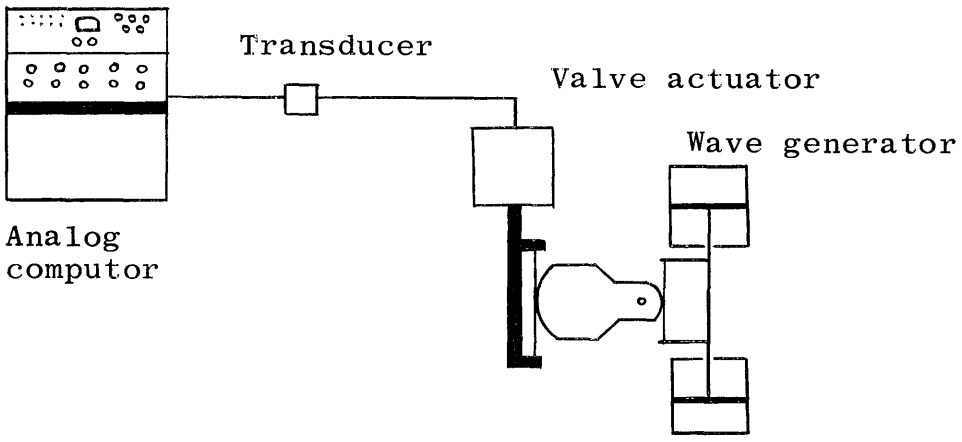

Figure 5: Generator and accessories

This pneumatic signal was applied to a Fisher, model 480-30, valve actuator. The resulting sinusoidal motion of the valve actuator was transmitted by a 4:1 lever arm to a rod connecting two, model 10-100, Bellowfram plastic cylinders. The completed apparatus is shown in Photographs 1 and 2 of Appendix II. Figure 6 shows the problem-board set up on the analog computor used to generate the electrical sinusoidal signal.

The frequency of the composition wave leaving the wave generator will always equal the frequency of the sinusoidal motion applied to the common piston rod. The amplitude of the composition wave depends, however, in the following manner upon the radian frequency, w, applied to the common piston rod, the volume, V, displaced in one cycle, and the volumetric flow rate, q_i, to each cylinder:

$$\text{Amplitude} = \frac{wV}{q_i} \qquad (13)$$

Therefore, if the amplitude of the composition wave presented to the silica gel bed is to remain constant during any one experiment, the value of V must be kept inversely proportional to the frequency. This was accomplished by changing the amplitude of the electronic signal which consequently changed the total length of travel of the common piston rod.

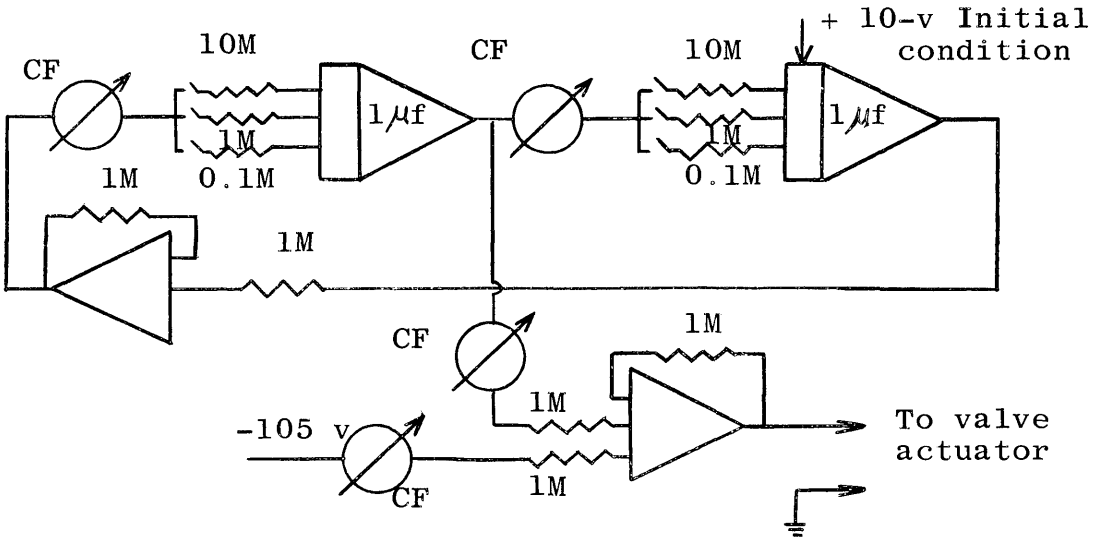

Coefficient potentiometer (CF)

Figure 6: Computor circuit for sinewave generator

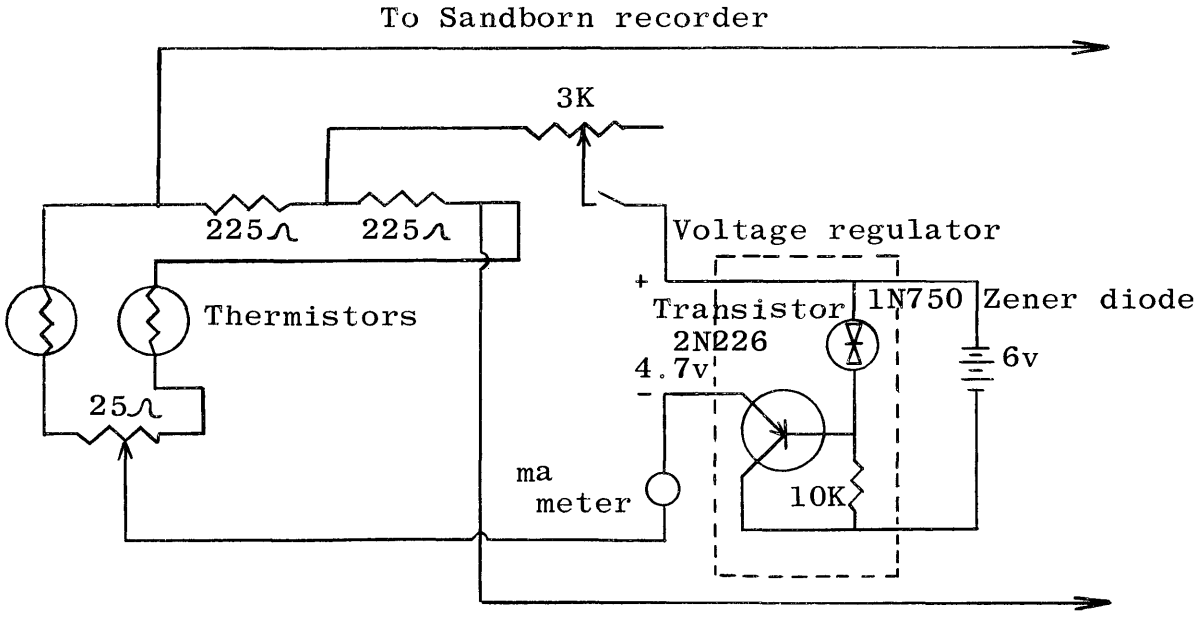

Figure 7: Bridge circuit for thermistors

Composition- and Temperature-Measurement Systems

Each composition measurement was made by using thermistor cells consisting of two matched Fenwall, model G 112, bead thermistors located in small cavities in a brass block. A stream of pure propane was introduced into one of these cavities (reference cell) and a stream of the binary gas mixture to be analyzed was introduced into the other (sensing cell). The thermistors were connected into a bridge circuit as shown in Figure 7.

As a consequence of its sinusoidal composition variation, the binary gas mixture exhibited a sinusoidal variation in its thermal conductivity. This variation in thermal conductivity caused a sinusoidal variation in the bead temperature of the sensing cell. Because thermistors are resistances with high negative-temperature coefficients of resistance, this latter variation imparted a sinusoidal voltage variation to the bridge output in direct proportion to the composition variation of the binary gas mixture. The bridge output signal is complicated, however, if variations in pressure, temperature, or flow exist because thermistors are also capable of measuring these quantities. The output signal of the bridge was amplified by a Sandborn, model 150-1500, low-level d-c amplifier and recorded on a Sandborn, model 54, 4-pen recorder.

Temperature measurements were made by locating 36-gauge iron-constantan thermocouples midway, both radially and

longitudinally, in the silica-gel beds. Figure 8 schematically represents the temperature-measurement system.

A Honeywell, model 2 HLA-9R, amplifier was used to preamplify the temperature signal before it entered the Sandborn amplifier-recorder system. Its output signal was complicated with some 60 cps noise. This noise necessitated the use of the first-order lag-filter shown in Figure 8. This filter was built on the problem board of the Donner analog computor.

Silica-Gel Beds

The kinetics of propylene-propane adsorption were to be studied using differential beds, so that longitudinal changes in temperature, pressure, and composition in the beds would be negligible. A flow rate to bed weight ratio of 10 cc/sec-gm was assumed to be sufficient to provide the above; consequently, six beds were constructed as shown in Figure 9. This assumption, however, was shown to be valid only over a portion of the frequency range studied.

All beds contained 1.02 gm of silica gel and approximately 9.3 gm of 8/12-mesh sand, except one which contained only the 9.3 gm of 8/12-mesh sand. This latter bed was used to determine the frequency response of the whole system minus any silica gel. All of the gel and sand used was dried to constant weight at 130°C. The particle sizes of the gel used were 14/20, 8/12, 6/8, 4/6, 3/4 mesh.

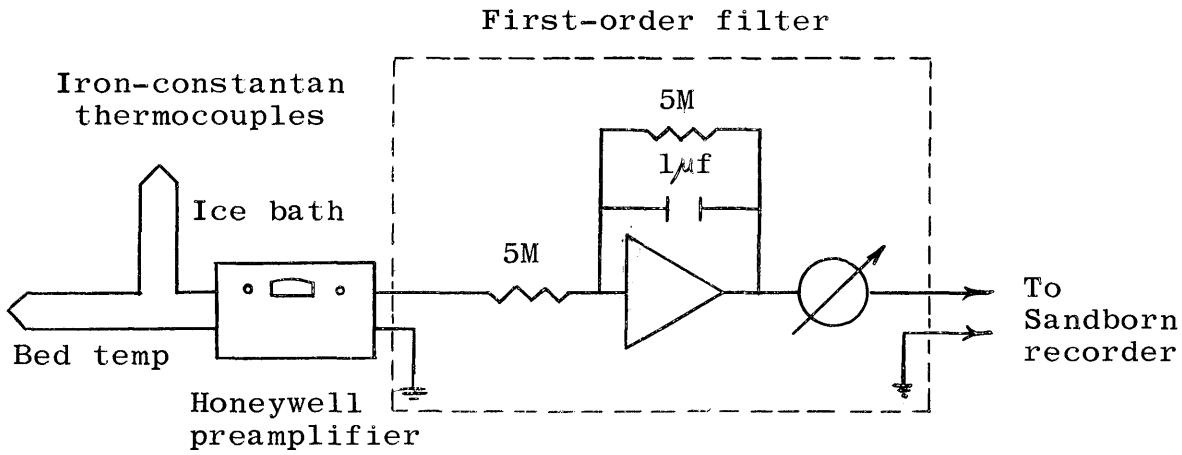

Figure 8: Temperature-measurement system

Diameter of reactor - 25/32 in. i.d.
Length of reactor: Sand bed - 25/32 in.
All gel beds - 1.0 in.

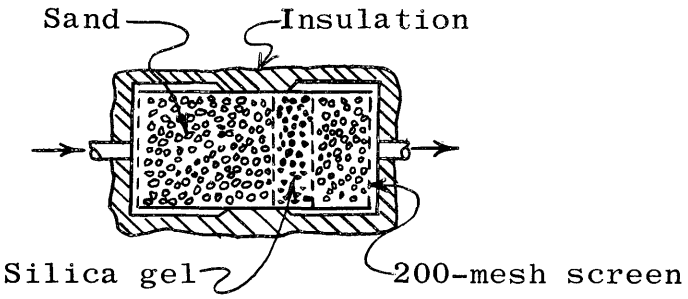

Figure 9: Typical gel bed

EXPERIMENTAL PROCEDURE

The experimental procedure consists of three operations: warm-up, analysis, and standardization.

Warm-Up

All of the electrical equipment was turned on one hour before starting an analysis to obtain stabilization of all the circuitry. The 6-volt storage battery used to supply the constant current through the thermistors was stabilized by placing a 2K ohm resistor across the output terminals of the voltage regulator shown in Figure 7.

Equal flows of propylene and propane through the system were established by blocking off the propylene stream at the composition generator and then adjusting the Moore flow controller in the propane stream until a flow of one half the desired total flow could be measured at the outlet of the system. The propylene stream was adjusted in a like manner. The combined streams produced an equal-molar mixture

flowing throughout the system since the downstream resistances of the two flow controllers were equal. Thirty minutes was allowed for the gel to become saturated with the mixture and for the bed and input gas-phase temperatures to equalize. The reference stream and the input and output thermistor streams were adjusted to 1.0 cc/sec.

The thermistor circuits were connected to the output of the voltage regulator and one milliamp of current was established in each circuit by adjusting the 3K ohm resistors (Figure 7). Thirty minutes was allowed for the currents to stabilize after the calibration step below.

With the outputs of the thermistor circuits connected to the Sandborn d-c amplifier-recorder systems and with the signals set at zero, obtained by opening the switches in the thermistor circuits, each amplifier-recorder system was calibrated as follows:

a. The zero suppression switch was set to off.

b. The attenuator was set to off and the position control adjusted to center the recorder stylus.

c. The attenuator was advanced to X1. The calibration button was pressed intermittently and the sensitivity control adjusted for a stylus deflection of two centimeters.

d. The attenuator was again turned to off, the zero suppression switch was set to on, and the switch in the thermistor circuit was closed.

This procedure resulted in a calibration of 100 micro-volts per centimeter of stylus deflection at an attenuation of X1.

The temperature measurement system was connected as shown in Figure 8 with the gain of the Honeywell preamplifier set at 10^4. The voltage representing the difference in temperature between the ice bath and the average bed temperature was noted and then partly zero suppressed at the preamplifier. The potentiometer at the outlet of the filter was set for a gain of 1.5×10^{-2}.

Because only two d-c amplifier-recorder systems were available and one of them had to be used to measure the input composition at all times, one amplifier-recorder system had to be used to measure both the output composition and the bed temperature. Instead of changing the calibration alternately to accommodate the output composition and bed temperature measurements, the above calibration procedure was repeated for the temperature-measurement system, except that the sensitivity control was not changed. The stylus deflection was noted (usually 1.55 cm) and all temperature measurements were multiplied by a correction factor (usually 2.00/1.55).

The air supply to the Fisher transducer and valve actuator system was turned on. The computor was placed in the reset mode which supplied a current of 3 milliamps to the transducer to center the valve actuator's piston rod at mid travel. Then the composition generator was connected to the valve actuator.

The warm-up operation was then completed, and the frequency-response analysis of a silica-gel bed could be started.

Analysis

The values for the resistances and potentiometers on the analog computor were set to produce a composition wave of a desired frequency and an amplitude variation of ±3.3 mole percent. The thermistor circuits were connected to the amplifier-recorder systems, the attenuators were set at X1, and the styli were centered with the zero suppression controls. Then the computor was switched from reset mode to compute mode. When five complete cycles for the input and output composition comparison had been recorded, the computor was switched back to reset mode. The output thermistor circuit was disconnected at the amplifier and replaced by the temperature-measurement circuit. Five complete cycles for the input composition and bed-temperature comparison were recorded in the same manner except that the

attenuator for the temperature circuit was set at X10 (1 milli-volt/centimeter of stylus deflection).

The frequency-response analysis of the silica-gel bed was complete when data had been recorded for a span of frequencies between 0.20 and 30.0 cpm.

Standardization

Reference lines representing the equal-molar mixture were obtained on the recorders at an attenuation of X10. Then the attenuators were turned to off. The propylene stream was blocked off at the composition generator, and a stream of pure propane flowing at a rate equal to that of the mixture was established in the system. The flow rates of the reference stream and the input and output thermistor streams were adjusted to 1.0 cc/sec. Then the thermistor outputs were recorded at an attenuation of X10. This procedure was repeated with propylene flowing through the system.

The standardization was complete when the voltage differences between the equal-molar mixture and the pure streams were obtained.

RESULTS

Experimental studies were made on five gel beds and one sand bed at two mass velocities. The frequency ranges covered in these analyses were from 0.20 to 30 cpm. The deviations of the input composition waves were ± 3.3 and ± 3.8 mole percent around equal-molar mixtures of propylene and propane. The average bed temperature for each run was $76.2 \pm 1.1^{\circ}F$. The bed pressures were 638 ± 4 and 668 ± 4 mm Hg for the low and high mass velocities, respectively.

Twelve frequency response analyses were made in all. Each of the five different particle sizes were analyzed at the low mass velocity to study the effects of particle diameter. Three beds were analyzed a second time to determine reproducibility. Then two gel beds were analyzed at the high mass velocity to study the effects resulting from changes in this parameter.

The Bode plots on the succeeding pages and Tables 6-17 in Appendix II represent the final results of this thesis.

G g/cm^2-sec	D_p cm	No. of Runs	Re_p
4.60×10^{-3}	0.0975	2	5.4
4.60×10^{-3}	0.184	1	10.2
4.60×10^{-3}	0.278	2	15.4
4.60×10^{-3}	0.390	1	21.6
4.60×10^{-3}	0.585	2	32.4
4.60×10^{-3}	sand	1	--
9.20×10^{-3}	0.0975	1	10.8
9.20×10^{-3}	0.585	1	64.8
9.20×10^{-3}	sand	1	--

Table 3: Distribution of runs

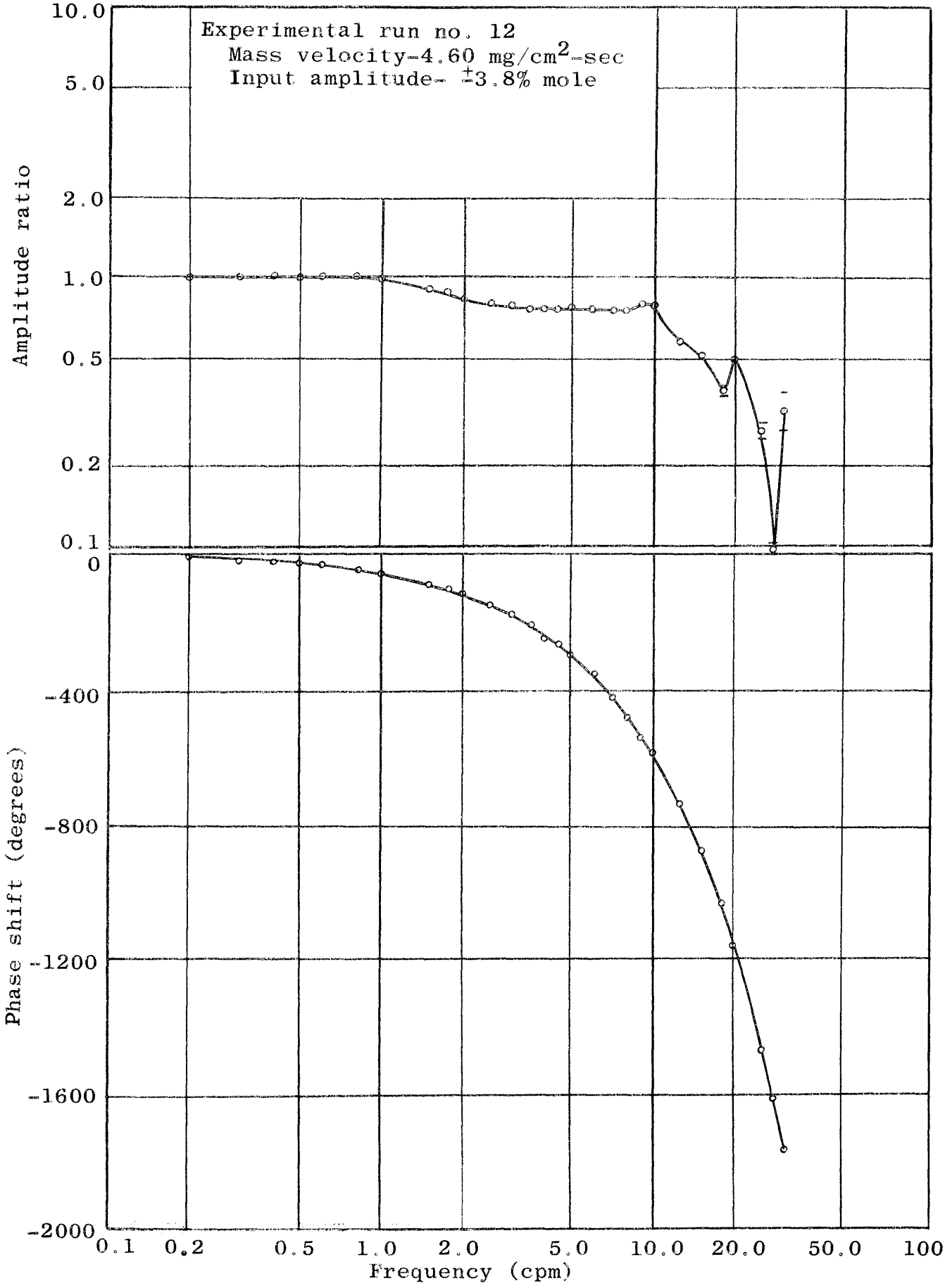

Figure 10: Composition vs frequency-sand bed at low flow

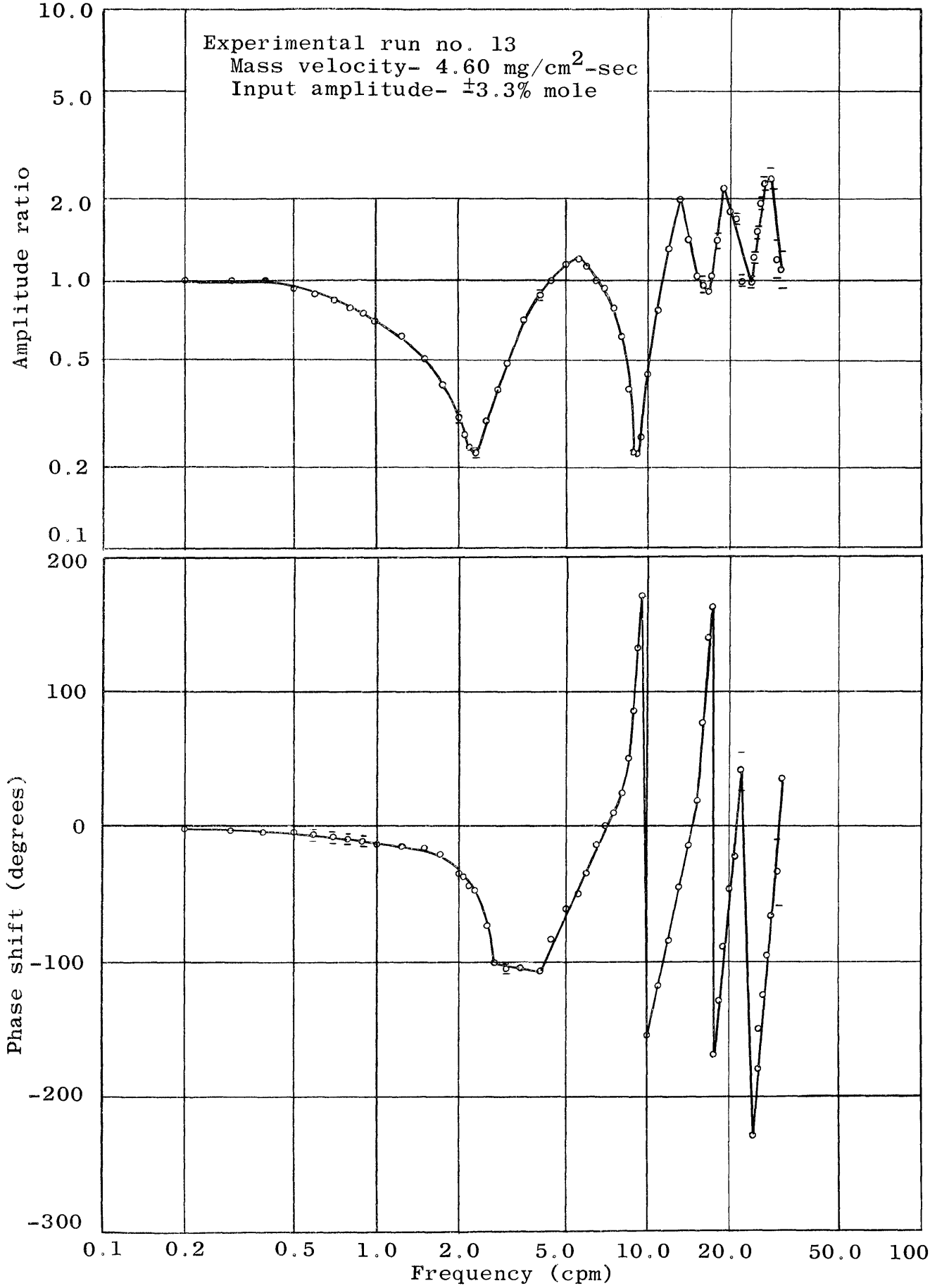

Figure 11: Composition vs frequency-14/20 mesh bed at low flow

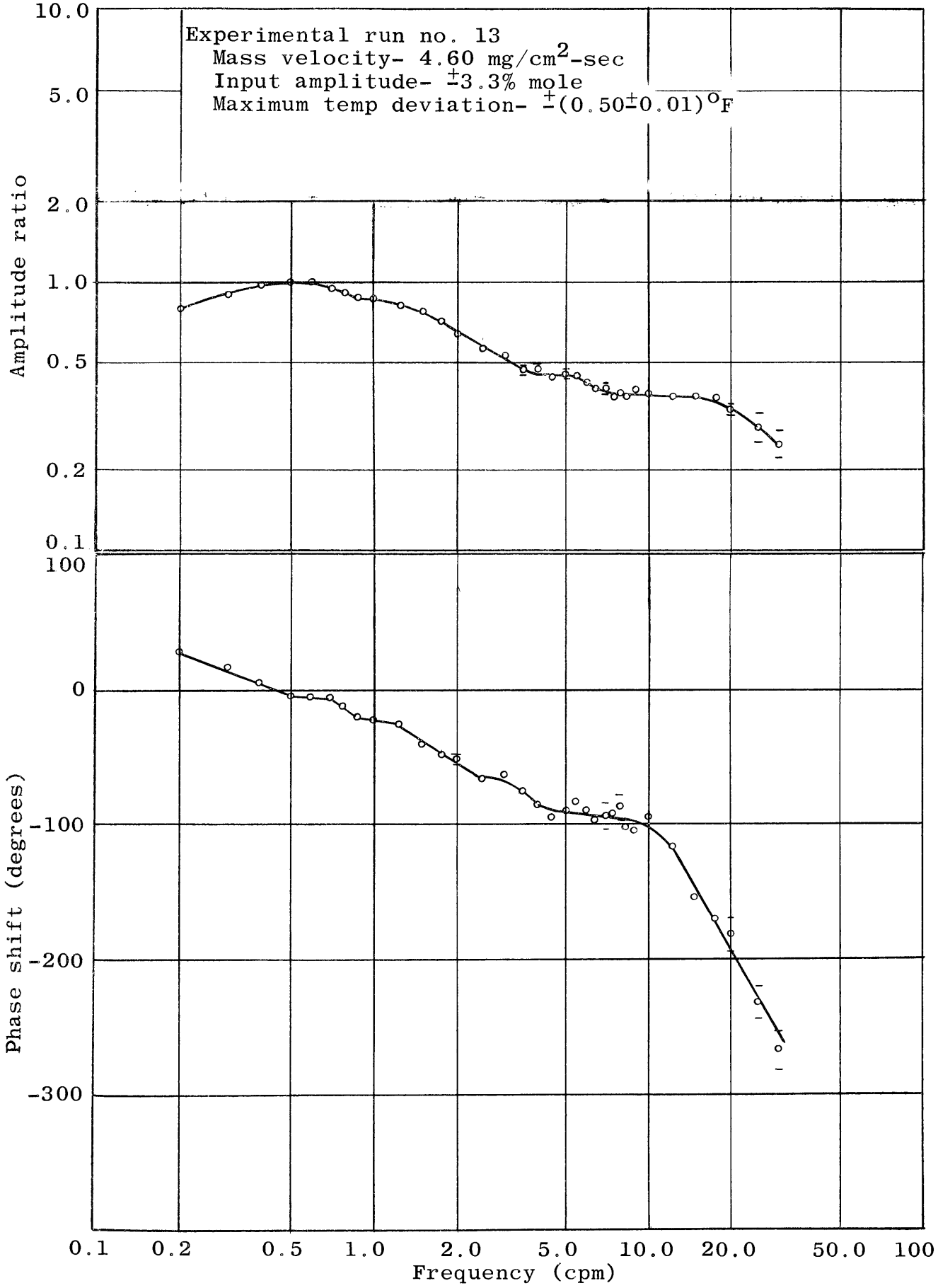

Figure 12: Temperature vs frequency-14/20 mesh bed at low flow

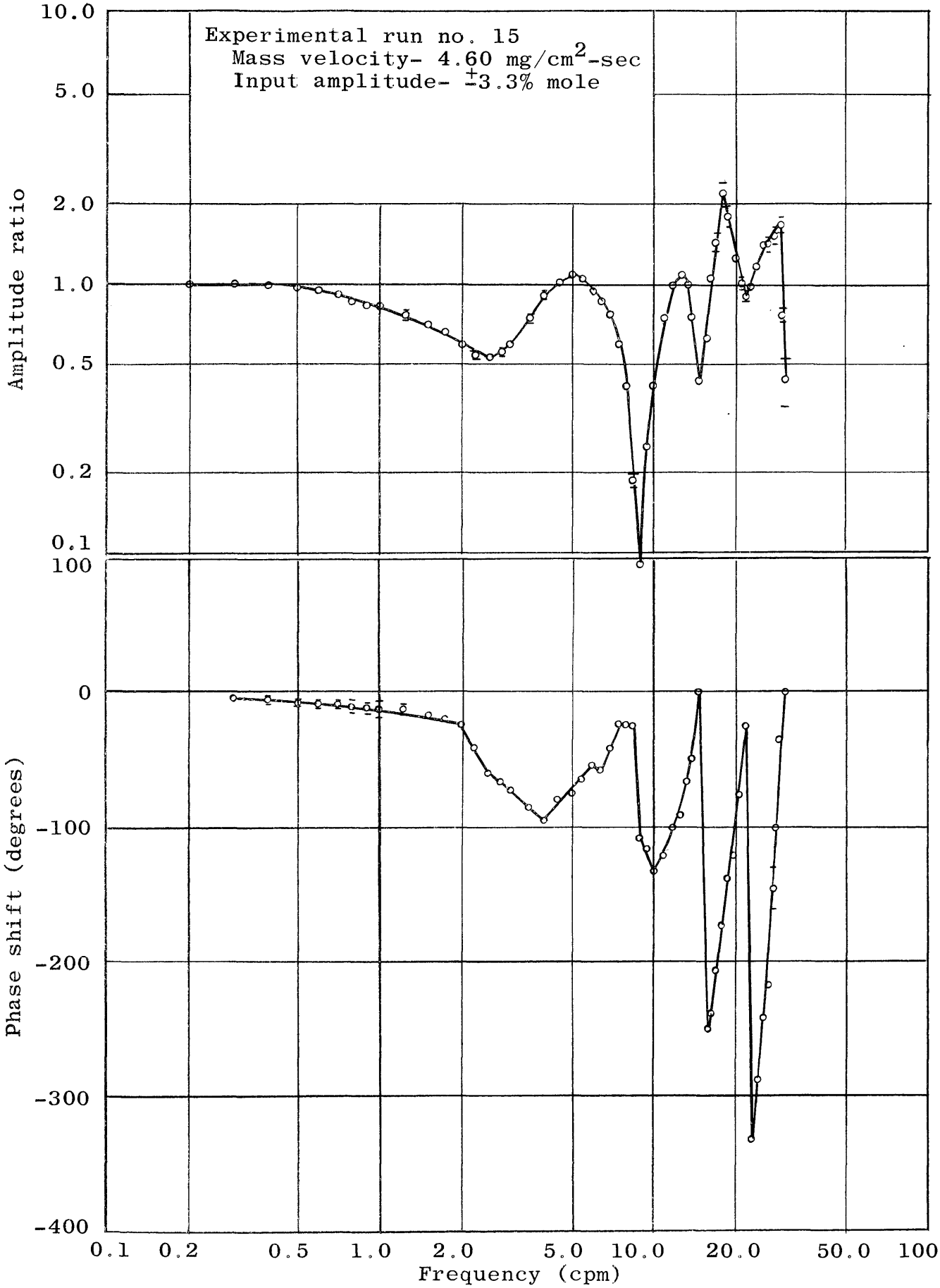

Figure 13: Composition vs frequency-6/8 mesh bed at low flow

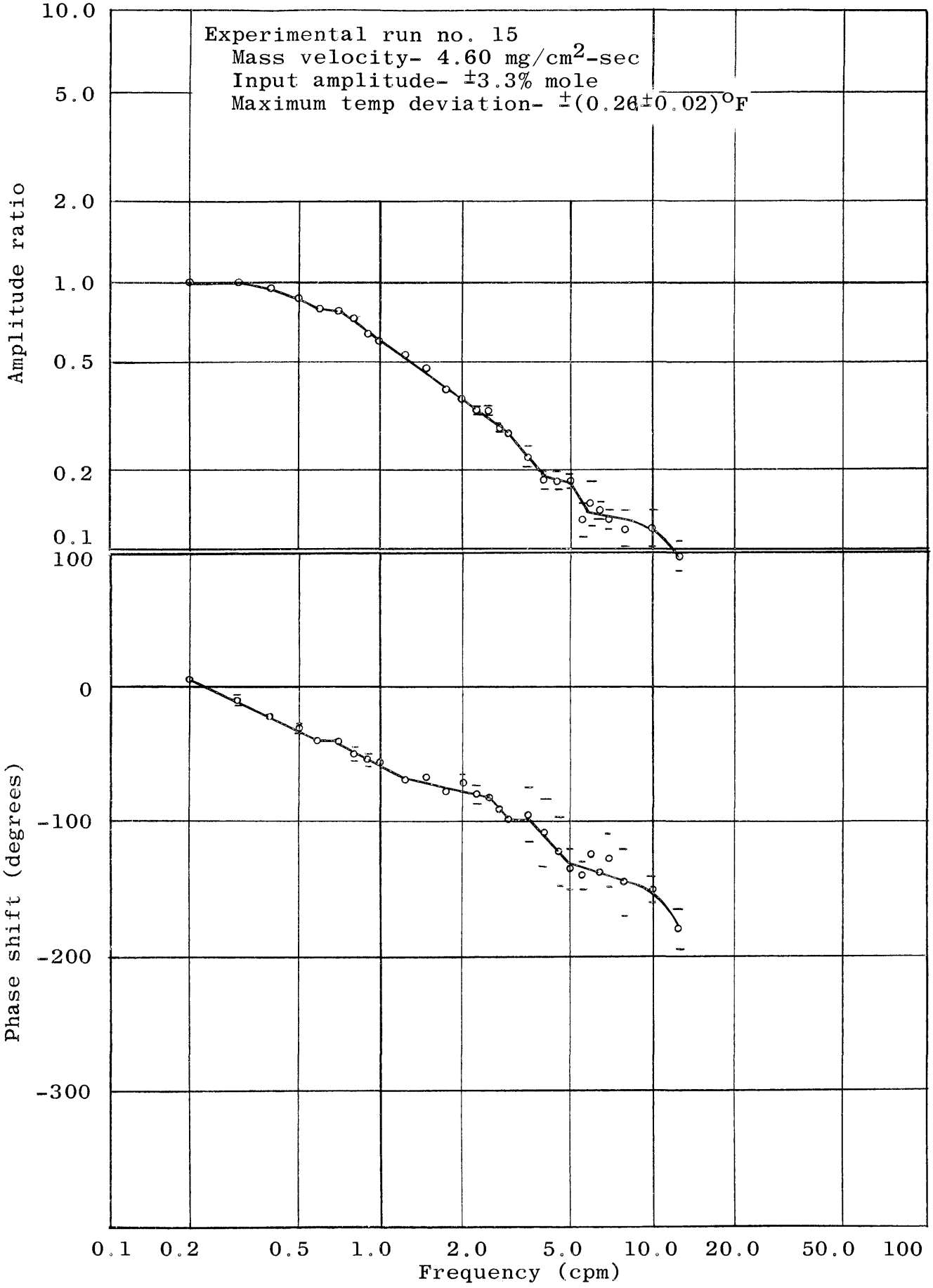

Figure 14: Temperature vs frequency-6/8 mesh bed at low flow

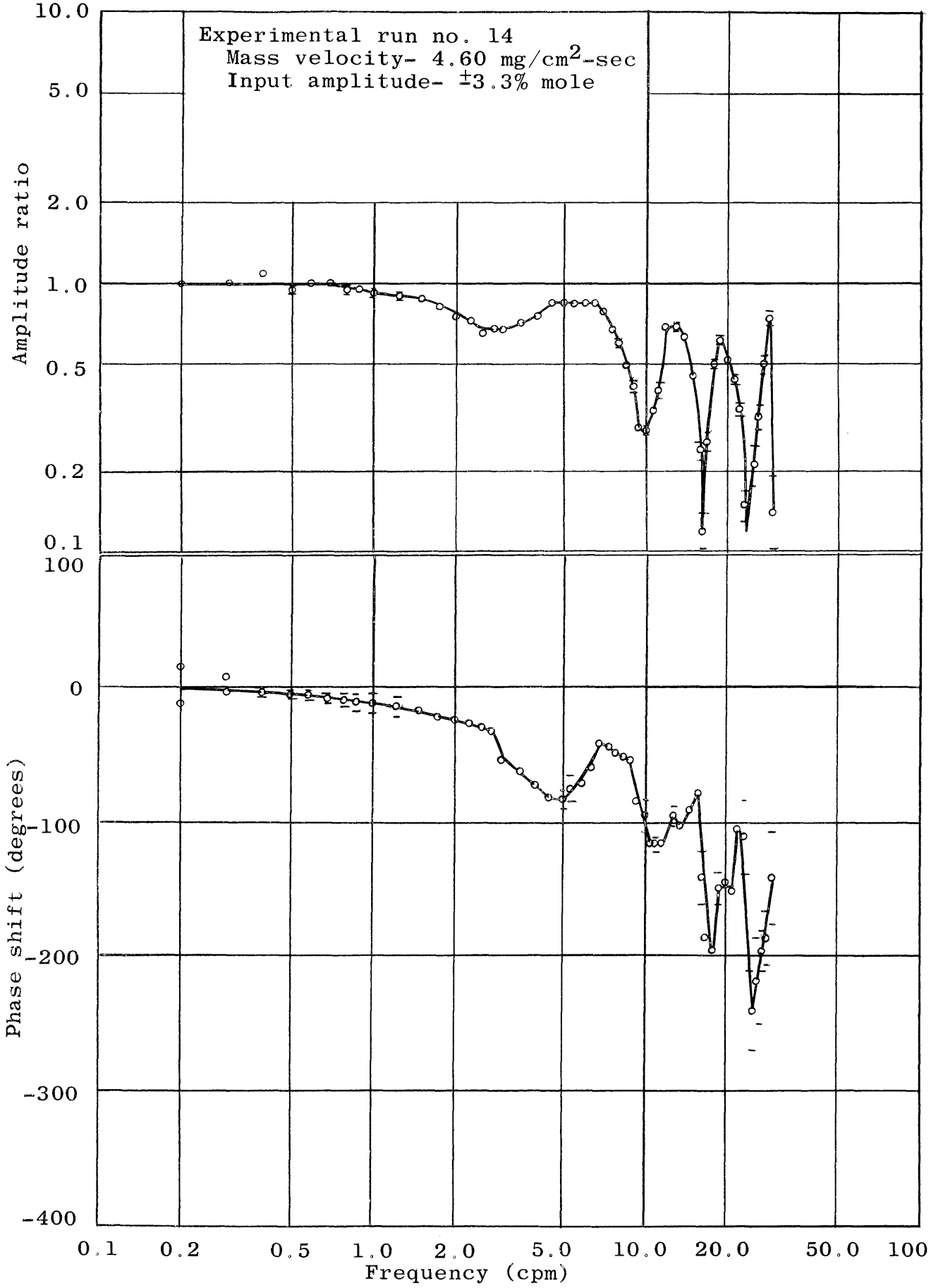

Figure 15: Composition vs frequency-3/4 mesh bed at low flow

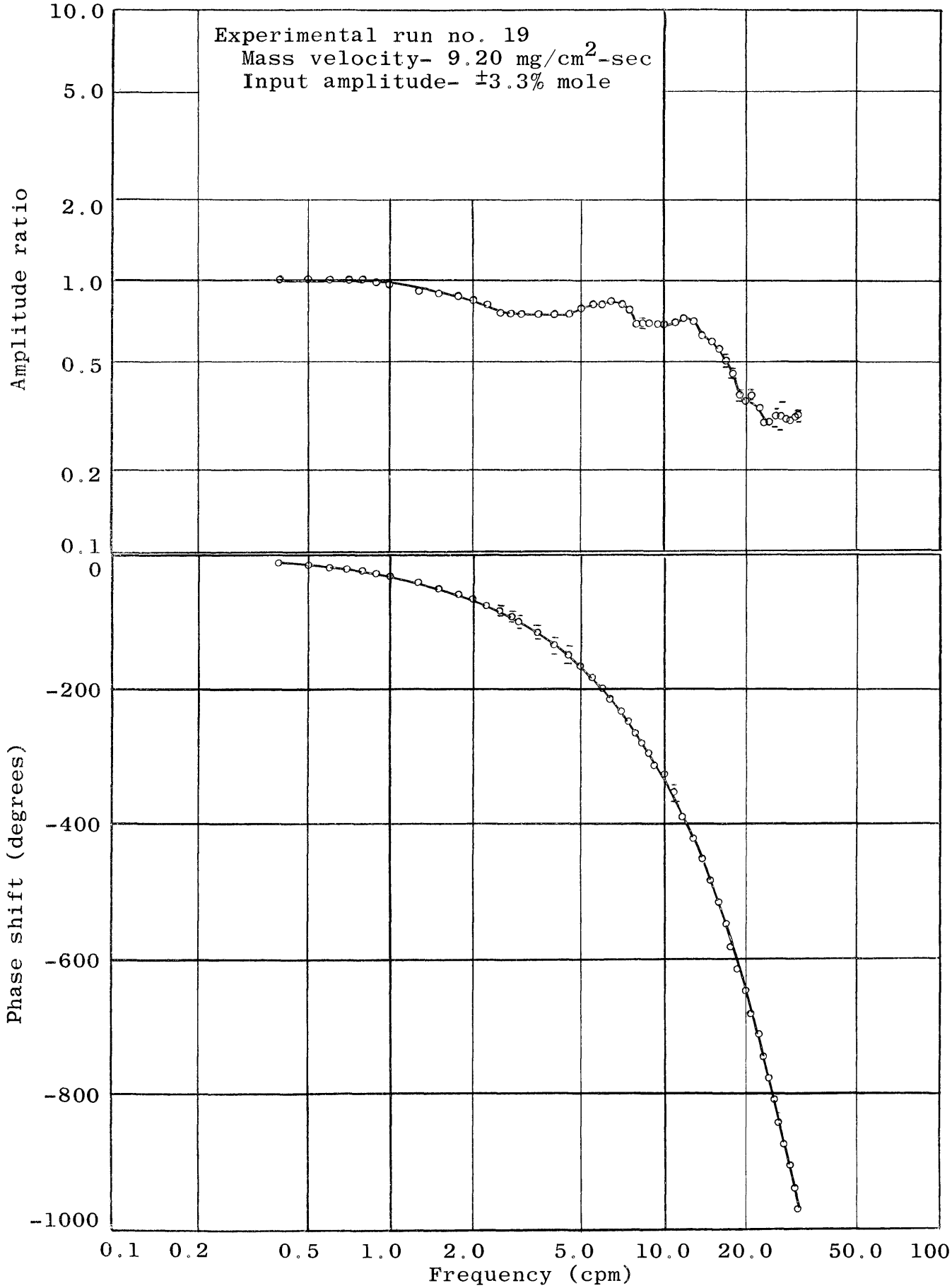

Figure 16: Composition vs frequency-sand bed at high flow

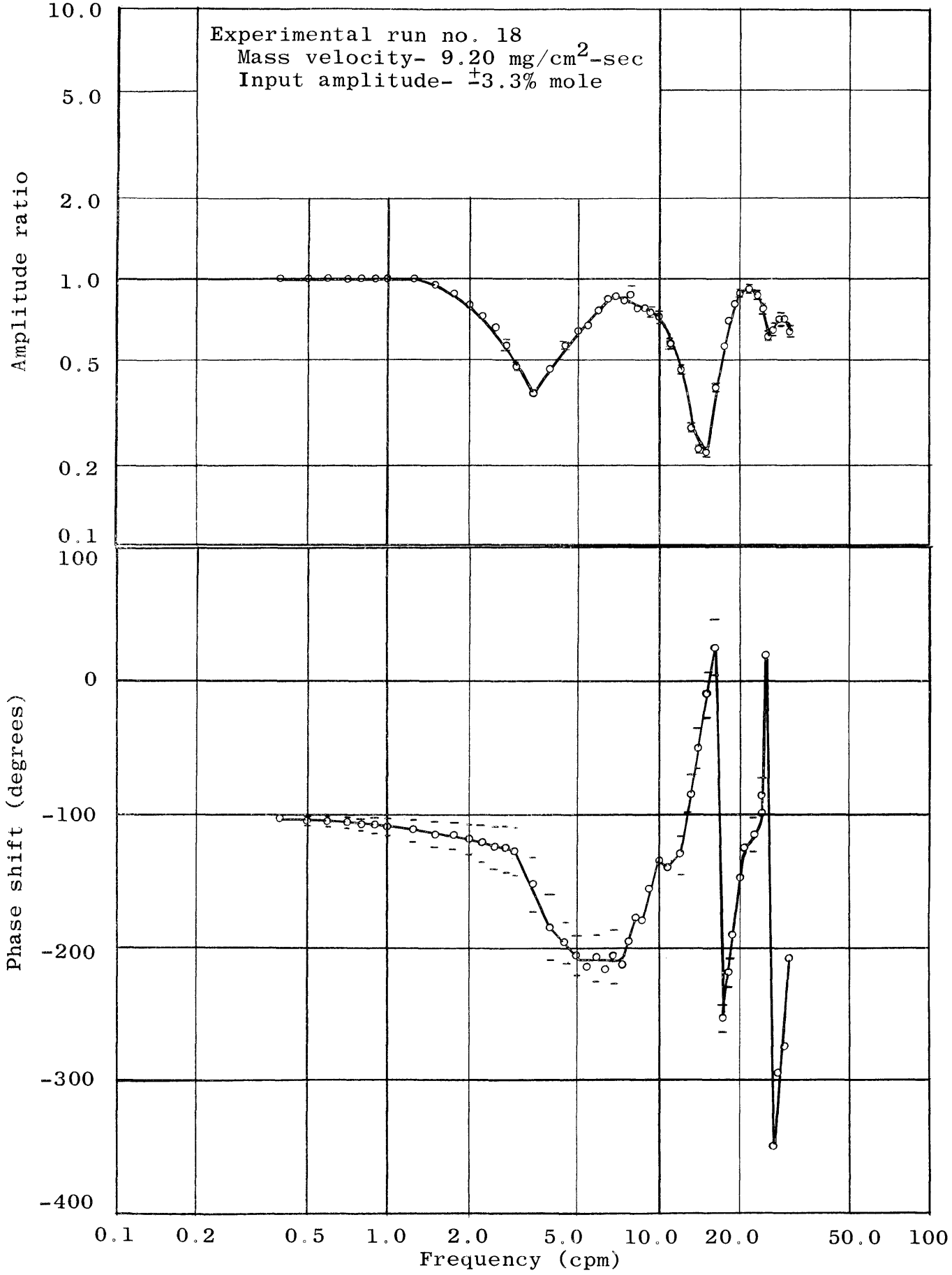

Figure 17: Composition vs frequency-14/20 mesh bed at high flow

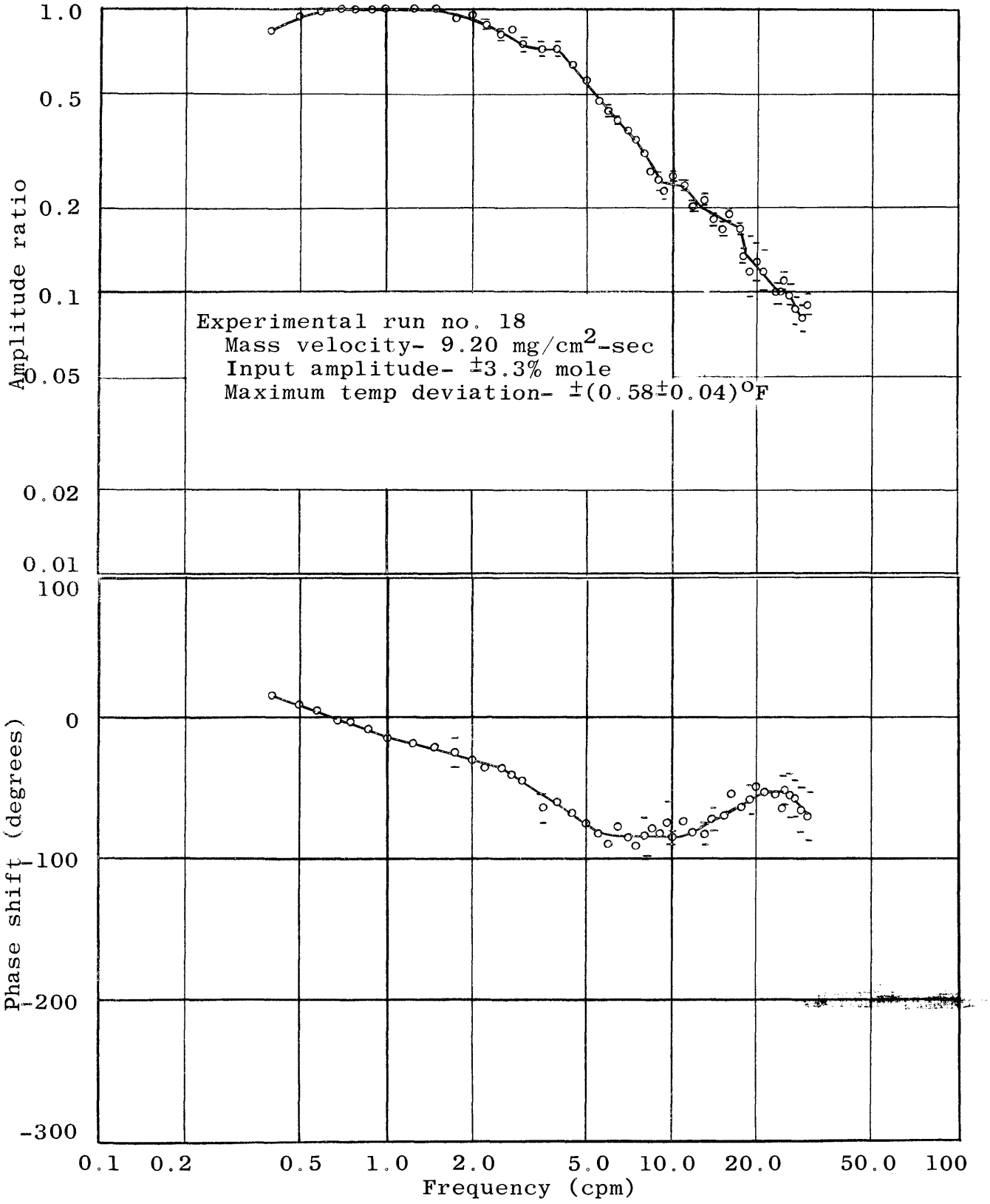

Figure 18: Temperature vs frequency-14/20 mesh bed at high flow

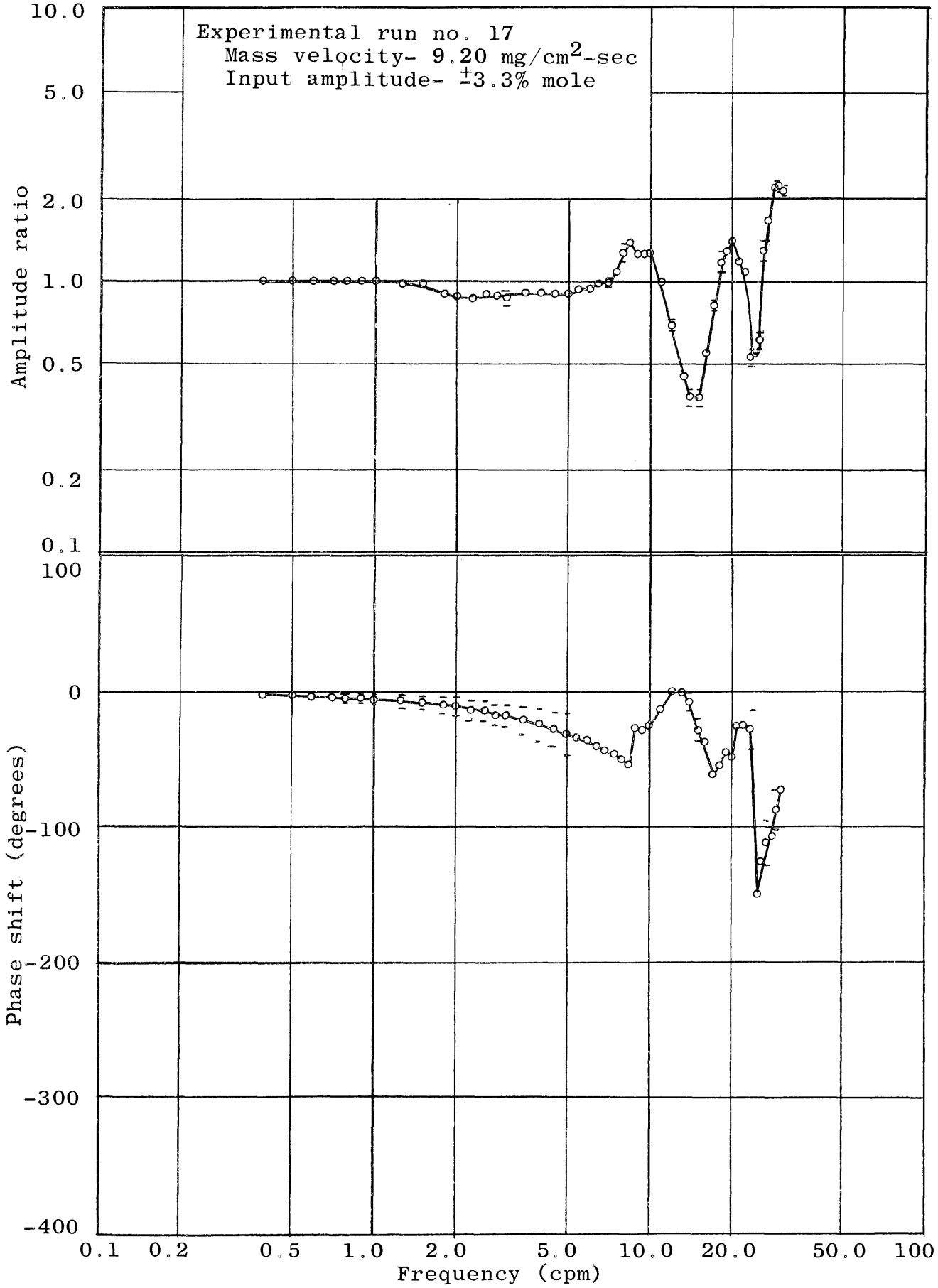

Figure 19: Composition vs frequency-3/4 mesh bed at high flow

DISCUSSION OF RESULTS

The results of this thesis are not extensive enough to provide definite conclusions concerning the variations in the rate-controlling mechanisms with variations in the particle size and in the mass velocity. The duplication of the runs on the 3/4-, 6/8-, and 14/20-mesh sizes at the low mass velocity shows that the frequency response characteristics for adsorption systems composed of propylene-propane over silica gel are definitely repeatable. Consequently, the results are discussed in a heuristic manner to aid future development of this thesis.

Ability of the Apparatus to Produce and Measure Sinusoidal Composition Variations

The sinusoidal composition waves produced by the apparatus were of varied quality. At low frequencies the input wave was complicated by noise owing to pressure fluctuations produced at the composition-wave generator.

This condition resulted in very inaccurate low-frequency phase lag measurements. These pressure fluctuations did not complicate the output wave owing to the smoothing of the system, nor did they complicate the input wave at high frequencies.

At high frequencies, greater than 7-10 cpm, the resistances to flow at the connections between the cylinders of the wave generator and their respective supply lines became critical. This resulted in a continual decrease in the amplitude of the composition wave as the frequency increased. This decrease had to be compensated for by increasing the stroke of the pistons. At frequencies greater than approximately 25 cpm, the amplitude of the composition wave became independent of the stroke of the pistons. Variations in the amplitude for any one frequency were also present, thereby decreasing the accuracies of the amplitude-ratio measurements at high frequencies. These latter variations probably were the result of the quality of the sinusoidal motion supplied to the pistons by the valve actuator. Also at high frequencies it was difficult to determine the multiple of complete cycles that the output composition wave lagged the input composition wave unless phase markers were made by superimposing impulses on the basic sine wave.

The voltage outputs representing the difference in composition between the equal-molar mixture and the pure streams of propylene and propane were found to be unequal. Therefore, the gas composition vs voltage output relationships for the thermistor cells are slightly non-linear. However, for the small changes in the gas-phase composition, the voltage deviations were equal around a center voltage representing the equal-molar mixture. Exceptions to this statement were the voltage deviations for the input thermistor cell at low frequencies. This is probably caused by the mixing of the gases being imperfect. Mixing occurred just prior to the input thermistor cell and was accomplished by connecting the pure streams from the composition generator to two legs of a tee-connector.

Amplitude and Phase Shift Characteristics of the Bed Temperature Measurement

For nearly all the frequencies studied the diffusional mechanisms occurred at essentially adiabatic conditions, p. 76. The noted nonlinearities in the composition phase shifts for the frequencies of 0.2 to 0.4 cpm are exceptions to the above statement. Because positive and corresponding negative temperature deviations around the average bed temperature were equal, equal-molar counter-diffusion of

propylene and propane was occurring. This occurrence means that the chosen sinusoidal deviations of ± 3.3 and ± 3.8 mole percent in the input composition were sufficiently small enough to obtain linearization of the studied adsorption systems and yet large enough to obtain significant results.

All amplitude ratios for the bed temperature were calculated using the maximum temperature deviation as the base amplitude. The input composition wave was used as the base for all phase shift measurements; therefore, a dead time is incorporated in all bed-temperature phase shifts. The magnitude of this dead time equals the time needed for the composition wave to travel from the input thermistor cell to the thermocouple location. This dead time should be the only phase lag noted at very low frequencies; however, it was noted at low frequencies that all temperature measurements were leading the input composition wave. The probable explanation for this is that the dead time for the material flowing through the input thermistor cell was larger than that for the material flowing through the bypass around the input thermistor cell. Consequently, any change in the gas phase composition will reach the bed before it is recorded by the thermistor cell. This error will not affect the phase lag vs frequency

relationships for the composition measurements. The reason is that the frequency-response characteristics of the two thermistor cells and supporting apparatus were determined and removed from the frequency-response characteristics of the gel beds plus the thermistor cells and the supporting apparatus.

The temperature amplitude ratio vs frequency plots, Figures 12, 14, and 18, show two major constant adsorption levels. A constant adsorption level is indicated by a constant value in the temperature amplitude ratio. The first level in each case occurs at low frequencies and can be associated with adsorption occurring on all internal and external surfaces. The increase in the temperature amplitude ratio at very low frequencies, 0.2 to 0.6 cpm, is the result of nonadiabatic conditions.

The occurrence of the second adsorption level depends upon the particle size and on the mass velocity. For the low mass velocity, the second level, occurring between the frequencies of 4 and 15 cpm, is invariant with particle size. The amplitude ratio at the second level for the 6/8-mesh bed is 2.9 ± 0.1 times smaller than that for the 14/20-mesh bed. Because the total external surface area of the 6/8-mesh bed is 2.85 times smaller than that for the 14/20-mesh bed, it seems that the second level of

adsorption can be associated with adsorption occurring on only the external surface of the particles. The second level of adsorption for the 14/20-mesh bed at the high mass velocity occurs between the frequencies of 9 and 18 cpm. However, the temperature amplitude ratio in this second adsorption level exhibits essentially two values, 0.18 and then 0.11.

Maximum Temperature Deviation, Low-Frequency Composition Dead Time, and Gel Capacity

The maximum adiabatic temperature deviation calculated, p. 75, using literature sources is $1.1\pm0.1^{o}F$ for a 1.02 g bed and for a ±3.3 mole percent composition deviation. The maximum total temperature deviations measured for the 14/20-mesh bed were 1.0 ± 0.1 and $1.2\pm0.1^{o}F$ for the mass velocities of 4.60 and 9.20 mg/cm^2-sec, respectively. Therefore, it can be concluded that this bed was exhibiting essentially maximum adiabatic adsorption.

The phase lag between the input and the output composition waves should be a constant dead time at frequencies small enough so that the resistance to mass diffusion between the bulk phase and the solid phase is not in effect. The magnitude of this dead time should equal the time needed for the bulk flow to supply the bed with sufficient material to saturate the gel. The calculated values, p. 78,

for the times needed by the low and high mass velocities to saturate the beds are 3.5 and 1.8 sec, respectively. The measured low-frequency dead times of 2 ± 1 and 1.5 ± 1.0 sec for the 14/20-mesh bed for the low and high mass velocities, respectively, are in fair agreement with the calculated values.

The maximum temperature deviation for the 6/8-mesh gel bed was $0.52\pm0.03^{\circ}F$. The lowest frequency studied in this thesis is probably in the range of frequencies in which the resistance to heat transfer from the interior of the particle to the bulk phase is effective. Therefore, the bulk-phase temperature measurement for this bed probably indicates a smaller temperature deviation than that occcurring in the particles of the bed. The measured composition low-frequency dead time of 2 ± 1 sec indicates that the average capacity of this gel was not different from that of the 14/20-mesh gel.

A sinusoidal variation in temperature could not be detected for the 3/4-mesh gel; therefore, the resistance to heat transfer between the particles and the bulk phase must be quite large. The measured low-frequency dead times of 2 ± 1 and 1 ± 1.0 sec for the low and high mass velocities do not indicate a change in the average capacity between this gel and the other two.

The amount of material that could be adsorbed in each half cycle, p. 75, is 0.0975 mgmoles if the adsorption processes had been carried out at an isothermal condition of 76.2°F, the average bed temperature for all the runs. The total change in the equilibrium adsorption capacity for a temperature deviation of 1.1°F is 0.02 mgmoles, p. 75. Therefore, it can be concluded for the adiabatic conditions studied that the change in the total equilibrium adsorption capacity in each half cycle was approximately 20 percent of the amount that could be adsorbed if the system were isothermal. This change in the equilibrium adsorption capacity would tend to decelerate the flow of mass from the bulk phase to the solid phase during half of the cycle and accelerate the flow of mass during the other half cycle. Consequently, an inductance effect is inherent in the fixed-bed adsorption systems studied in this thesis.

Comparison of the Calculated and Experimental Plots of the R/R_i Ratio vs Particle Diameter

The plots, Figure 20, of the experimental R/R_i ratio vs particle diameter show slopes of 1.1 and 1.4 for the low and high mass velocities, respectively. The calculated R/R_i ratio vs particle diameter plots show slopes of 1.8 and 2.2 for the low and high mass velocities, respectively. Therefore, it can be concluded that the diffusion length

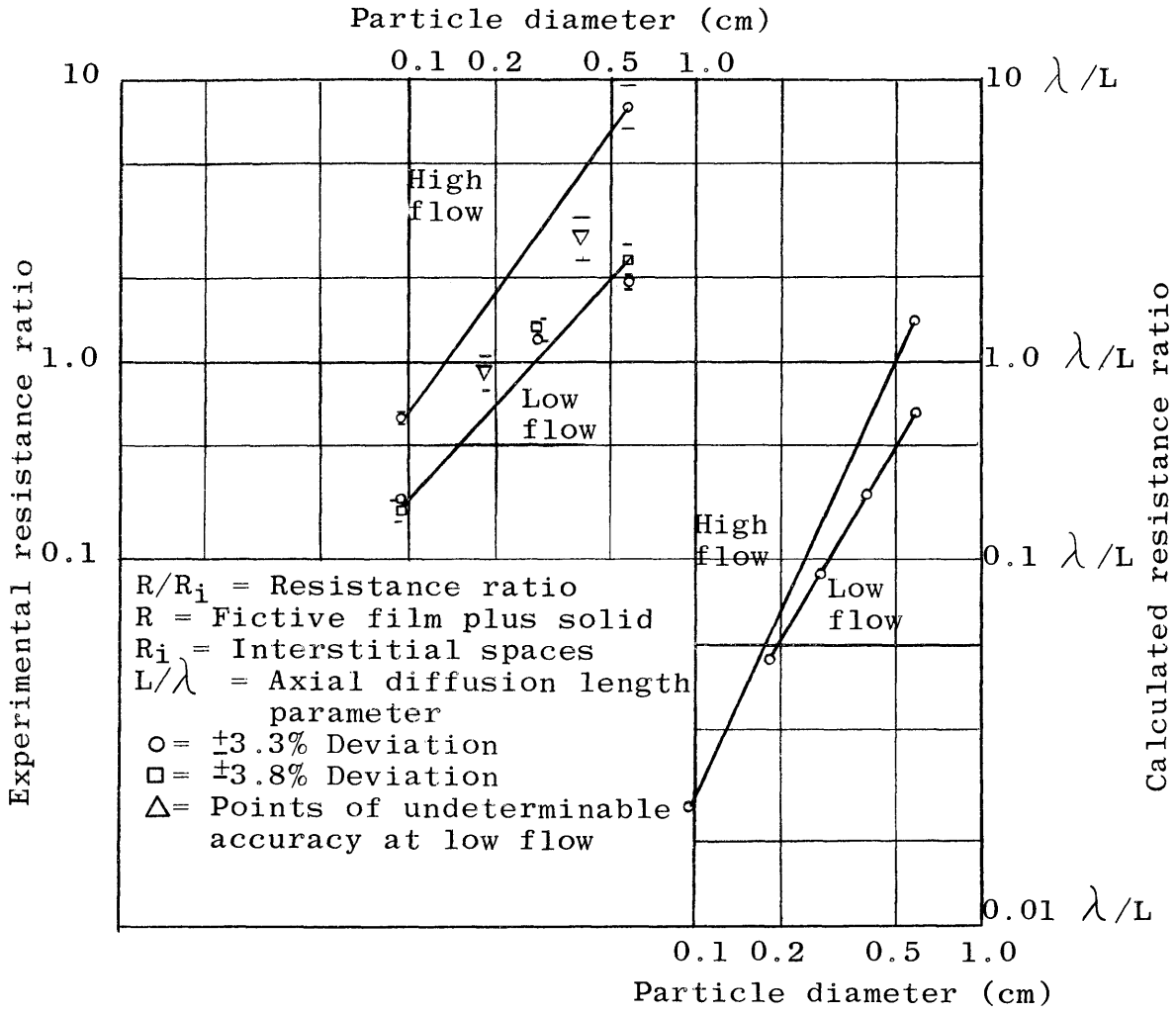

Figure 20: R/R_i ratios vs particle diameter

parameter, L/λ, is not invariant of particle diameter because the calculated and experimental slopes for each mass velocity are not equal. The following table shows the values for the axial diffusion length parameter obtained by dividing the experimental values of the R/R_i ratio, Table 18, by the respective calculated values of the R/R_i ratio, Table 2.

G	D_p	L/λ
gm/cm^2-sec	cm	cm^{-1}
4.60×10^{-3}	0.278	7.2 ± 0.5
4.60×10^{-3}	0.585	3.2 ± 0.6
9.20×10^{-3}	0.0975	24 ± 1
9.20×10^{-3}	0.585	5.2 ± 1.2

Table 4: Values for the diffusion length parameter

Since the labyrinth factor, λ, is dependent only on the manufacturing procedure, it is assumed to be independent of particle diameter. Therefore, it can be concluded from the above table that the diffusion length, L, is inversely proportional to 1.0 ± 0.2 power of the particle diameter and directly proportional to the 0.68 ± 0.10 power of the mass velocity.

Frequency of First Resonance on Composition Amplitude Ratio vs Frequency Plots

The frequency at which the first resonance occurs for the low mass velocity seems to be independent of particle size or at the very most increases by a factor of 1.1 for each of the particle size increases, Figure 21. However, when the mass velocity was increased by a factor of 2, the frequency at which the first resonance occurred was essentially unchanged for the 3/4-mesh gel and increased by a factor of 1.5 for the 14/20-mesh gel. Therefore, it might be concluded that the interior particle mechanisms controlling the inductance-capacitance property of the 3/4-mesh gel are nearly independent of the mass velocity and that the film mechanisms controlling the inductance-capacitance property of the 14/20-mesh gel are mass velocity dependent.

Frequency Difference Between Successive Resonant Frequencies on the Composition Amplitude Ratio vs Frequency Plots

The frequency difference between successive resonant frequencies at the low mass velocity was a constant value of approximately 7 cpm and invariant with particle size, Figure 21. At the high mass velocity the difference between the successive resonant frequencies were higher by a factor of 1.6 or 11 cpm, except the difference between the first

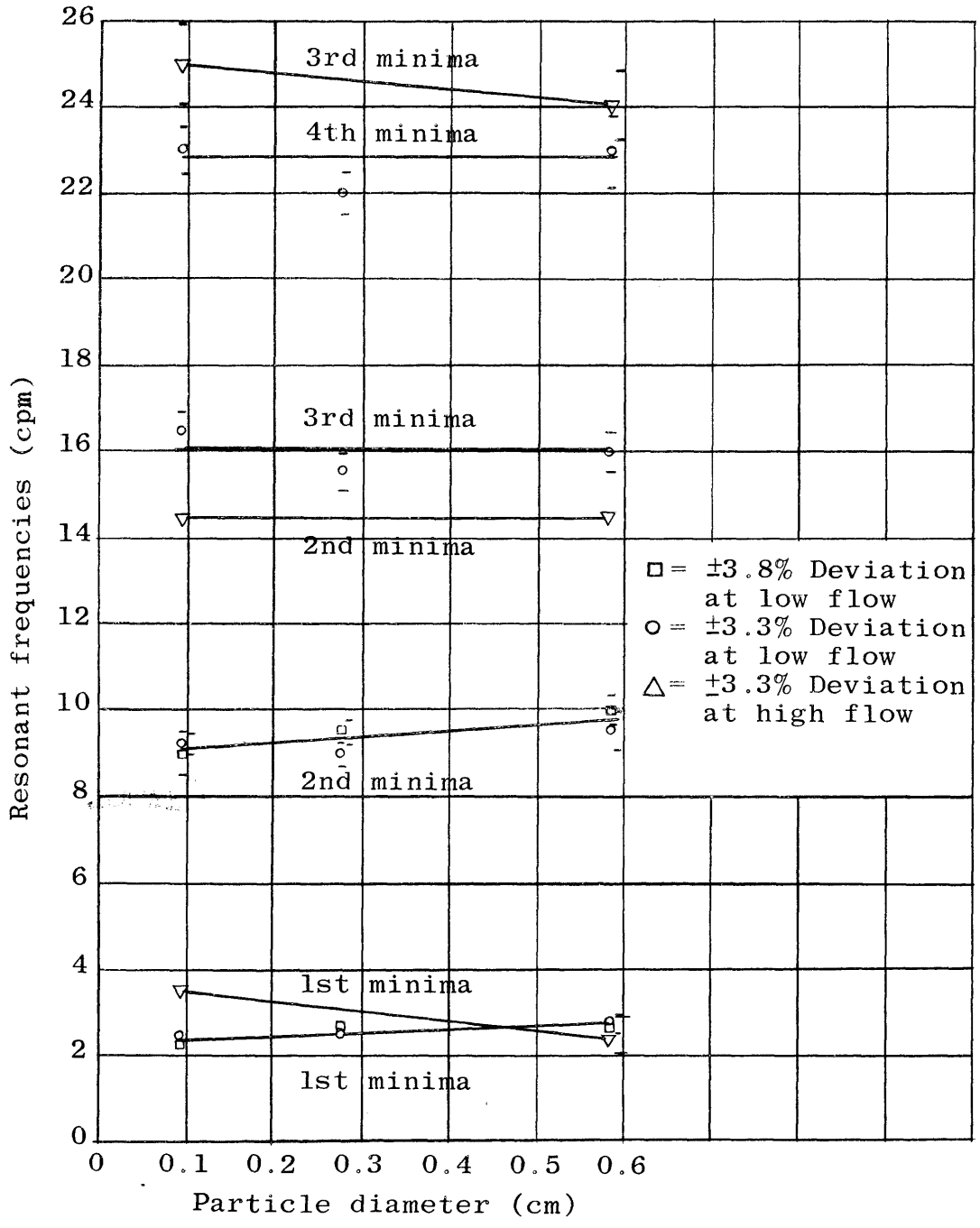

Figure 21: Resonant frequencies vs particle diameter

and second resonant frequencies for the 3/4-mesh gel. It increased to approximately 12 cpm because the first resonant frequency for this gel did not vary with the increase in the mass velocity. Therefore, it might be concluded that the first resonant frequency, at least for the 3/4-mesh gel, is caused by a different phenomenon than that causing the rest of the resonant frequencies.

Composition Phase Shift Characteristics

It has already been noted that at low frequencies the phase shift between the output and input composition waves for each bed represents a constant dead time. As the frequency of the input composition wave is increased, a frequency is reached at which the phase shift becomes greater than that of the low-frequency dead time. The only exception to the last statement is exhibited by the 3/4-mesh gel at the high mass velocity which showed a decrease in phase shift from its low-frequency dead time. With increasing frequency, the phase shift for each bed tends to level out and then increases to resonate with the maximum value occurring at approximately the minimum value of the amplitude ratio. The first resonant frequency for the phase shift occurs at the second resonant frequency for the amplitude ratio. This experimental result substantiates the conclusion

of the last section: that the first resonant frequencies on the amplitude ratio plots are the result of phenomenon different from the rest of the amplitude resonances.

The frequency at which the phase lag deviates from the low-frequency dead time is inversely proportional to the adsorption-time constant. The adsorption-time constant is a measure of the time needed for a gel to obtain equilibrium with the inlet bulk fluid when a step change in the latter has been made. Figure 22 shows the obtained relationship between the deviation frequency and particle size for the two mass velocities. For the low mass velocity the deviation frequency seems to increase only slightly with any increase in the particle size. The deviation frequency increased by a factor of 1.6 ± 0.1 for the 14/20-mesh gel for an increase in the mass velocity by a factor of 2. The deviation frequency increased by a factor of 3.2 ± 0.2 for the 3/4-mesh gel for the given increase in the mass velocity. However, as already noted, the phase shift for this gel deviated in an opposite manner compared to the rest of the runs.

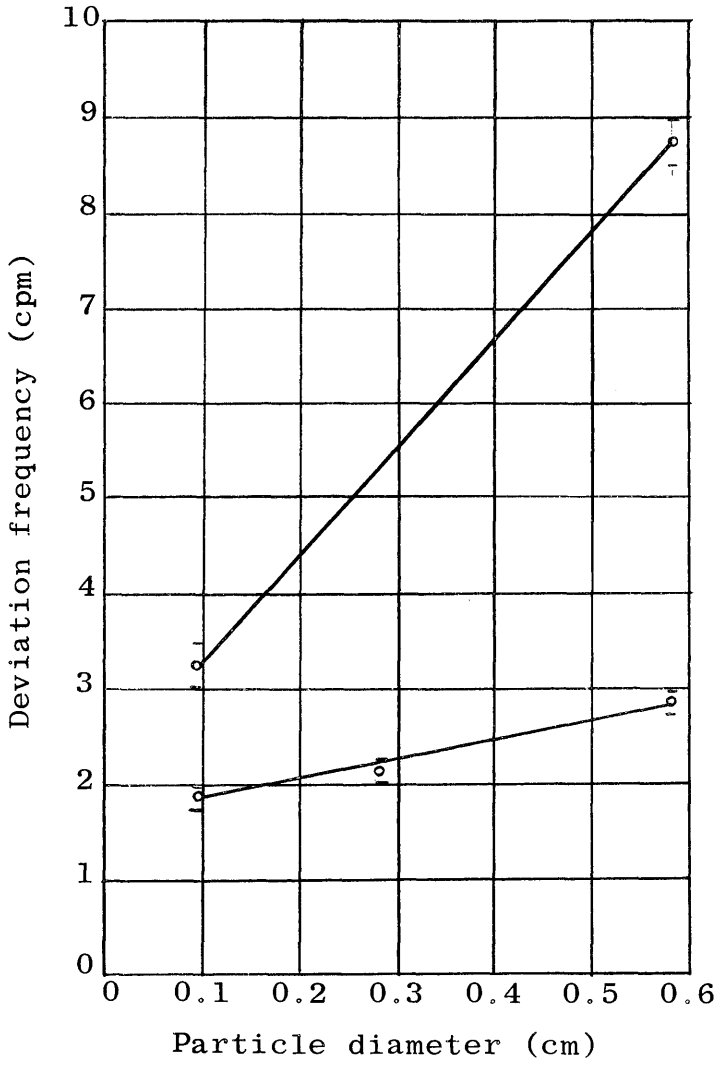

Figure 22: Deviation frequency vs particle diameter

CONCLUSIONS AND RECOMMENDATIONS

A successful experimental apparatus has been developed for obtaining the frequency-response characteristics of fixed-bed adsorption systems. This apparatus was used to discover details of adsorption kinetics of propylene-propane exchange on silica gel not previously described in the literature. However, more experimentation must be carried out before the hypotheses made between the obtained frequency response characteristics and the parameters describing the rate-controlling mechanisms can be brought together into a coherent theory. Recommendations by the author for future work fall under two general classifications: improvement of the experimental apparatus, and extension of the variables studied.

Improvement of the Experimental Apparatus

The accuracies of the composition low-frequency phase lag and of the high-frequency amplitude ratio

measurements could be improved by redesigning each piston of the composition generator as shown in Figure 23. The diameters of the input and output tubing will depend upon the flow rates studied; however, the input tubing must be smaller than that of the output tubing. This arrangement insures that any pressure fluctuations resulting from expansion or compression of the gases in one of the pistons will be transmitted to the mixing tee where they will be nulled by the opposite pressure fluctuations produced in the other piston.

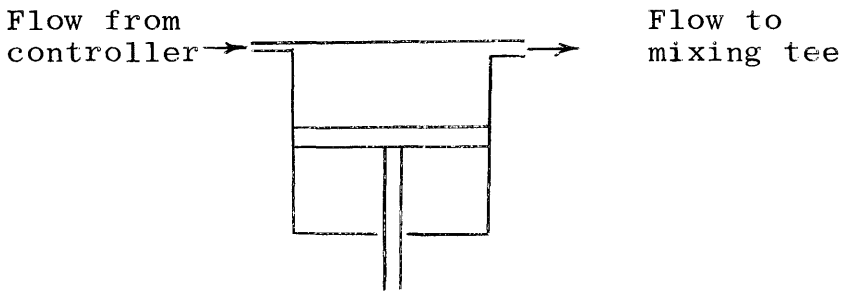

Figure 23: Piston design for composition generator

More accurate amplitude ratio and phase-lag measurements in general could be made by the use of an X-Y plotter. In this case the output signal, either composition or temperature, is added to the input signal and the resulting signal attached after sufficient magnification to one axis of the X-Y plotter. A pure sine wave and a pure cosine

wave from the analog computor are combined in the following manner:

$$a \sin(wt) + b \cos(wt) = \sin(A + wt)$$

where $a^2 + b^2 = 1$

$$A = \tan^{-1}(b/a)$$

This signal is attached to the other axis of the X-Y plotter and the constants a and b varied until the curve drawn on the plotter becomes a straight line. This condition means that the phase lag between the two functions attached to the X-Y plotter is zero. The value of A then is the phase lag in radians between the input composition signal and the output composition or temperature signal. The slope of the straight line will be proportional to the amplitude ratio.

The quality of the sinusoidal motion delivered to the rod connecting the two pistons was limited by the precision of the positioning mechanism to a resolution of ±0.001 in. according to manufacturing specification. This precision could have been a contributing factor in the noisy composition waves produced. An infinite resolution linear-motion transducer attached to the connecting rod would provide a measure of the quality of the above sinusoidal motion, and could be used to attempt an improvement in the resolution.

More information concerning the amount of and rate of adsorption could be obtained if particle surface temperatures were determined instead of bulk-phase temperatures. Thirty-six-gauge thermocouples could easily be inserted a small distance inside a single gel particle without appreciably changing the total volume of the particle. However, spherical particles would be a necessity to insure that the particle chosen for the temperature measurement would represent the average particle size. The phase lags of particle surface temperatures would indicate the depth of material penetration in the particle. However, the complications described earlier concerning the dead time of the thermistor cells would have to be eliminated, probably by reducing the volumes of the thermistor cells.

It would be more convenient if the temperature measurement filter were built separate from the analog computor because the computor must be in the compute mode for the filter to be operative. This arrangement makes the measure of the average bed temperature difficult.

Extension of the Variables Studied

It is believed that only the first resonances on the composition Bode plots are related to the beds functioning like differential adsorption systems. Consequently, future experimentation should be directed toward isolating the

first resonance of each bed from the other resonances. This could be accomplished by either reducing the size of the beds or by increasing the bulk flow rates. Either procedure in effect will increase the frequency range over which the beds are of the differential type.

The proposed relationship between the ratio of R/R_i and the amplitude ratio at the first resonance was checked using literature values for R and R_i, Equations 5, 8, and 10; however, these literature values are not very reliable for the range of Reynolds numbers, 5.4 to 64.8, used in this thesis. Consequently, the above proposed relationship should be checked for all the beds used in this thesis at Reynolds numbers greater than 50.

It is not known definitely whether the capacitance and the inductance properties of fixed-bed adsorption systems can be described using separate parameters or whether they must be lumped into one parameter. However, the following description suggests a method by which values for the capacitance and inductance parameters could be obtained.

As has been noted capacitance is defined as follows:

$$\text{Capacitance (C)} = \frac{I}{dE/dt} = \frac{dQ/dt}{dE/dt}$$

where I = Current or mass flow

Q = Charge or mass stored

E = Potential

The time rate of change of potential needed in capacitance determinations equals the time rate of change of the bulk-phase composition at frequencies low enough so that the resistance to mass diffusion between the bulk phase and the solid phase is not in effect. Because in adiabatic systems the bed temperature is directly related to the amount of material stored, the time rate of change of the mass stored is proportional to the time rate of change of the solid-phase temperature. At high frequencies the potential causing mass storage can not be related to the bulk-phase composition nor the particle surface composition because the resistance to mass diffusion is primarily in the solid phase. Therefore, it seems doubtful that capacitance parameters can be calculated at high frequencies.

The following equation defines the inductance parameter.

$$\text{Inductance (L)} = \frac{E}{dI/dt} = \frac{E}{d^2Q/dt^2}$$

It has already been noted that the time rate of change of mass flow from the bulk phase to the solid phase is a result of changes in the bed temperature and consequent

changes in gel capacity. Therefore, the instantaneous bed temperature is proportional to the potential needed in any inductance calculations. The time rate of change of mass flow from the bulk phase to the solid phase is proportional to the derivative of the time rate of change of the bed temperature.

BIBLIOGRAPHY

Campbell, D. P., 1958, Process dynamics: New York, John Wiley and Sons, Inc., 316 p.

Deisler, P. F., Jr., and Wilhelm, R. H., 1953, Diffusion in beds of porous solids, measurement by frequency response techniques: Industrial and Engineering Chemistry, v. 45, p. 1219-27.

Fahien, R. W., and Smith, J. M., 1955, Mass transfer in packed beds: A.I.Ch.E. Journal, v. 1, March, p. 28-37.

Hougen, O. A., and Watson, K. M., 1947, Chemical process principles, part 3 - kinetics and catalysis: New York, John Wiley and Sons, Inc., p. 805-1107.

Keyes, J. J., Jr., 1955, Diffusional film characteristics in turbulent flow: dynamic response method: A.I.Ch.E. Journal, v. 1, September, p. 305-311.

Lewis, W. K., Gilliland, E. R., Chertow, B., and Cadogan, W. P., 1950, Adsorption equilibria hydrocarbon gas mixtures: Industrial and Engineering Chemistry, v. 42, July, p. 1319-32.

Mantell, C. L., 1951, Adsorption: New York, McGraw-Hill Book Company, Inc., 634 p.

Maxwell, J. B., 1957, Data book on hydrocarbons: New York, D. Van Nostrand Company, Inc., 259 p.

Pauls, A. C., Olt, R. G., Romano, R. C., and Stanton, J. S., 1960, Instrumentation's role in reactor response studies: ISA Journal, v. 7, November, p. 46-51.

Perry, J. H., 1950, Chemical engineers' handbook: New York, McGraw-Hill Book Company, Inc., 1942 p.

Rosen, J. B., and Winsche, W. E., 1950, The admittance concept in the kinetics of chromatography: The Journal of Chemical Physics, v. 18, December, p. 1587-92.

Shimoda, E., (unpublished), Colorado School of Mines, Thesis No. T889.

Smith, J. M., 1956, Chemical engineering kinetics: New York, McGraw-Hill Book Company, Inc., 402 p.

Wheeler, A., 1951, Advances in catalysis: New York, Academic Press Inc., v. 3, p. 249-327.

Wilke, C. R., and Hougen, O. A., 1945, Mass transfer in the flow of gases through granular solids extended to low modified Reynolds numbers: Transactions of The American Institute of Chemical Engineers, v. 41, February, p. 445-451.

APPENDIX I

Tabulations of Useful Data

From this thesis

Mean bed temperature: $76.2 \pm 1.1^{\circ}F$ - $24.5 \pm 0.6^{\circ}C$

Atmospheric temperature: $79.1 \pm 1.1^{\circ}F$ - $26.1 \pm 0.6^{\circ}C$

Atmospheric pressure: 620 ± 4 mm Hg abs

Bed pressure at 10.0 cc/sec: 638 ± 4 mm Hg abs

Bed pressure at 20.0 cc/sec: 668 ± 4 mm Hg abs

From Hougen and Watson (1947, p. 1085)

Mesh size	Particle diameter
	cm
14/20	0.0975
8/12	0.184
6/8	0.278
4/6	0.390
3/4	0.585

From Lewis, Gilliland, Chertow, and Cadogan (1950, p. 1320-1323)

Propylene equilibrium ratio, $K_=$, at 25.0°C, 760 mm Hg, and for the equal-molar mixture: 0.67 ± 0.01

Capacity of silica gel for propylene, $N'_=$, at 25.0°C and 638 and 668 mm Hg, respectively: 2.05 and 2.10 mgmoles/ g bed

Capacity of silica gel for propane, N', at 25.0°C and 638 and 668 mm Hg, respectively: 1.32 and 1.38 mgmoles/ g bed

Empirical relationship between N, mgmoles adsorbed from a gas mixture per g bed, and N', mgmoles of pure gas adsorbed per g bed: $\sum N/N' = 1$

From Maxwell (1957, p. 89)

Specific heat of the equal-molar mixture at 76.2°F: 0.38 cal/g-°C

From Mantell (1951, p. 176)

Specific heat of silica gel: 0.22 cal/g-°C

Particle density of silica gel: 0.7 g/cc

Average pore diameter of silica gel: 4×10^{-7}cm

From Perry (1950, p. 371)

Viscosity of the equal-molar mixture at 76.2°F: 8.3×10^{-5} g/cm-sec

From Shimoda (unpublished)

Heat of adsorption of propylene on silica gel:

4.08 kcal/gmole

Heat of adsorption of propane on silica gel:

2.03 kcal/gmole

Gel Capacity and Relative Volatility

Propylene capacity of gel at 24.5±0.6°C and 653±15 mm Hg:

$$\ln \frac{N_{=}'}{(2.07\pm0.02)} = \frac{4.08 \frac{\text{kcal}}{\text{gmole}}}{1.98 \frac{\text{cal}}{\text{gmole-K}}} \left[\frac{1}{(297.7\pm0.6)} - \frac{1}{(298.2)} \right] \frac{1}{K}$$

$N_{=}' = 2.09\pm0.02$ mgmoles/g bed

Propane capacity of gel at 24.5±0.6 C and 653±15 mm Hg:

$$\ln \frac{N'}{(1.35\pm0.03)} = \frac{2.03}{1.98} \left[\frac{1}{(297.7\pm0.6)} - \frac{1}{(298.2)} \right]$$

$N' = 1.36\pm0.03$ mgmoles/g bed

Therefore, it can be concluded that the gel capacity will not vary more than 3 percent for the temperature and pressure fluctuations between the various runs.

Relative volatility, α, at 24.5±0.6°C, 653±15 mm Hg, and for the equal-molar mixture:

$$\ln \frac{K_=}{(0.67\pm0.01)} = \frac{4.08}{1.98}\left[\frac{1}{(297.7\pm0.6)} - \frac{1}{(298.2)}\right]$$

$K_= = \underline{0.66\pm0.02}$

$x_= = y_=/K_= = 0.50/0.66\pm0.02 = 0.76\pm0.02$

$$\alpha = \frac{(1-y_=)}{(1-x_=)} \cdot \frac{x_=}{y_=} = \frac{0.50}{1-(0.76\pm0.02)} \cdot \frac{(0.76\pm0.02)}{0.50}$$

$\alpha = \underline{3.2\pm0.3}$

Gel capacity in equilibrium with the equal-molar gas mixture:

$N_= = \alpha N(p_=/p) = (3.2\pm0.3)N$

$$\frac{(3.2\pm0.3)N}{(2.09\pm0.02)} + \frac{N}{(1.36\pm0.03)} = 1$$

$N = 0.44\pm0.02$ mgmoles/g bed

$N_= = 1.42\pm0.03$ mgmoles/g bed

$N_t = \underline{1.86\pm0.05 \text{ mgmoles/g bed}}$

Cross Sectional Area and Volume of Reactor

Cross sectional area $= \frac{\pi}{4} \times \left[\frac{25}{32}\right]^2 \times (2.54)^2 = \underline{3.10 \text{ cm}^2}$

Volume $= 3.10 \times \frac{17}{32} \times 2.54 = \underline{4.18 \text{ cc}}$

Mass Velocity and Reynolds Number

Molar volume at $26.1\pm0.6^{\circ}C$ and 620 ± 4 mm Hg:

$$V_m = \frac{RT}{P} = 62.36 \frac{\text{l-mm Hg}}{\text{gmole-K}} \times \frac{(299.3\pm0.6)K}{(620\pm4)\text{mm Hg}}$$

$V_m = 30.0 \pm 0.2$ l/gmole

Mass flow rate at 10.0 cc/sec:

$$q_{w-10} = 10.0 \frac{cc}{sec} \times \frac{mgmole}{(30.0 \pm 0.2)cc} \times 43 \times 10^{-3} \frac{g}{mgmole}$$

$$= (1.43 \pm 0.2) \times 10^{-2} \text{ g/sec}$$

Mass velocity at 10.0 cc/sec:

$$G_{10} = (1.43 \pm 0.02) \times 10^{-2} \frac{g}{sec} \times \frac{1}{3.10 \text{ cm}^2}$$

$$= \underline{(4.60 \pm 0.05) \times 10^{-3} \text{ g/cm}^2\text{-sec}}$$

Reynolds number at 10.0 cc/sec and for the 14/20-mesh gel:

$$Re_p = D_p G/\mu = \frac{0.0975\text{cm} \times 4.6 \times 10^{-3} \text{ g/cm}^2\text{-sec}}{8.3 \times 10^{-5} \text{ g/cm-sec}}$$

$$= \underline{5.4}$$

Density of Bulk Phase in Gel Bed

$$\rho_f = \frac{PM}{RT} = \frac{(653 \pm 15) \text{ mm Hg}}{62.36 \frac{\text{l-mm Hg}}{\text{gmole-K}}} \times \frac{43 \text{ g/gmole}}{(297.7 \pm 0.6)\text{K}} = \underline{1.52 \pm 0.03 \text{ g/l}}$$

Specific Heat of Gel System

c_p(gel) = 0.22 cal/g bed-^oC

c_p(adsorbed phase) = 0.38 cal/g-^oC x 43 g/gmole

x (1.86 ± 0.05)gmole/g bed

= 0.03 cal/g bed-^oC

Amount of bulk phase assuming void fraction of 0.4

$N_b = (4.18 \times 0.4)\text{cc/g bed} \times 1.52\text{mg/cc} \times 1/43\text{mgmole/mg}$

$= 5.9 \times 10^{-2}$ mgmole/g bed

$$c_p(\text{bulk phase}) = 5.9 \times 10^{-5} \frac{\text{gmole}}{\text{g bed}} \times 0.38 \frac{\text{cal}}{\text{g-}^\circ\text{C}} \times 43 \frac{\text{g}}{\text{gmole}}$$

$$= 9.6 \times 10^{-4} \text{ cal/g bed-}^\circ\text{C}$$

$$c_p(\text{total}) = 0.25 \text{ cal/g bed-}^\circ\text{C}$$

Maximum Amount Adsorbed for a ±3.3 Mole Percent Deviation in Bulk-Phase Composition and for Isothermal Conditions

By definition $x_{=} = \dfrac{\alpha y_{=}}{1 + (\alpha - 1)y_{=}}$

Then for $0.467 \leq y_{=} \leq 0.533$, $0.74 \leq x_{=} \leq 0.79$

$N_{=} = N = (1.86 \pm 0.05)\dfrac{\text{mgmole}}{\text{g bed}}\ (1.02)\text{g bed}\ (0.79-0.74)$

$= \underline{(9.5 \pm 0.2) \times 10^{-2} \text{ mgmole}}$

Amount Adsorbed and Temperature Deviation for a ±3.3 Mole Percent Deviation in Bulk-Phase Composition and for Adiabatic Conditions

Heat liberated on adsorption:

$4.08 - 2.08 = 2.05$ kcal/gmole

Average heat of adsorption for adsorbed material:

$H_{avg} = (4.08 \times 0.76) + (2.03 \times 0.24) = 3.6$kcal/gmole

Assume adiabatic adsorption, as a trial value, to equal 0.8 of the isothermal adsorption:

$(9.5 \pm 0.2) \times 10^{-2} \times 0.8 = (7.6 \pm 0.2) \times 10^{-2}$mgmole

$$H_{ad} = 2.05 \frac{cal}{mgmole} \times (7.6 \pm 0.2) \times 10^{-2} mgmole = 0.15 \pm 0.01 cal$$

$$\text{Temperature rise} = 0.15 \pm 0.01 cal \times \frac{g\ bed\text{-}^{o}C}{0.25\ cal} \times \frac{1}{1.02\ g\ bed}$$

$$= 0.59 \pm 0.04^{o}C$$

Change in gel capacity resulting from the rise in temperature:

$$\ln \frac{N_t}{(1.86)} = \frac{3.6 kcal/gmole}{1.98 cal/gmole K} \left[\frac{1}{(298.3)} - \frac{1}{(297.7)} \right] \frac{1}{K}$$

$N_t = 1.84$ mgmole

$\triangle N_t = 1.86 - 1.84 = 0.02$ mgmole

For the above assumption to be correct, the assumed amount of adiabatic adsorption plus the change in the gel capacity resulting from the temperature rise should be equal to the amount of isothermal adsorption.

$(7.6 \pm 0.2) \times 10^{-2} + 0.02 = (9.6 \pm 0.2) \times 10^{-2}$ mgmole

Therefore, the trial assumption is correct.

Amount of adiabatic adsorption = $\underline{(7.6 \pm 0.2) \times 10^{-2} mgmole}$

Adiabatic temperature rise = $\underline{1.1 \pm 0.1^{o}F}$

Proof That Adiabatic Adsorption is Occurring

Because the beds were insulated, the only way heat could have been removed from the system was by the heat capacity of the bulk flow. The bulk-phase temperature rise would equal that calculated in the last section if there were no resistance to heat

transfer between the solid phase and the bulk phase. The rates of heat removal assuming no heat-transfer resistance are:

$$Q_{10} = 0.38 \frac{cal}{g\text{-}^oC} \times 1.43\times10^{-2} \frac{g}{sec} (0.59\pm0.04)^oC$$

$$= (3.2\pm0.2)\times10^{-3} cal/sec$$

$$Q_{20} = (6.4\pm0.4)\times10^{-3} cal/sec$$

The times needed for the bulk flows to completely remove the adiabatic heat calculated in the last section are:

$$t_{10} = (0.15\pm0.01)cal \times \frac{1\ sec}{(3.2\pm0.2)\times10^{-3} cal}$$

$$= 48\pm7\ sec$$

$$t_{20} = 24\pm3\ sec$$

The Bode plots of the amount of heat removed vs frequency of the input composition wave would be first-order lag functions. The corner frequencies of which will be proportional to the above calculated times.

$$1/t_{10} = \frac{60\ sec/min}{2\pi\ rad/sec \times 48\pm7\ sec/rad}$$

$$= 0.20\pm0.03\ cpm$$

$$1/t_{20} = 0.40\pm0.06\ cpm$$

The amount of heat removed can be considered negligible and the studied systems adiabatic for frequencies greater by a factor of 10 than the above corner frequencies. This means that the studied frequencies of 0.2-2.0 cpm and 0.4-4.0 cpm for the 10.0 and 20.0 cc/sec flow rates, respectively, would be in a nonadiabatic region. However, nonadiabatic regions would be characterized by nonlinearities in the composition phase shifts. Nonlinearities were not noted for frequencies greater than 0.4 cpm. Therefore, it can be concluded that the resistances to heat transfer are not negligible for any of the systems studied and that adiabatic conditions were realized for most of the frequencies studied.

Time Needed for the Bulk Flows to Supply Sufficient Material For Adiabatic Gel Saturation

Molar flow rate:

$$q_{m-10} = \frac{(1.43 \pm 0.02) \times 10^{-2} \text{ g/sec}}{43 \text{ g/gmole}} \times 10^3 \frac{\text{mgmole}}{\text{gmole}}$$

$$= (0.326 \pm 0.004) \text{ mgmole/sec}$$

$$q_{m-20} = (0.652 \pm 0.008) \text{ mgmole/sec}$$

Percent of molar flow available for supplying material to the gel is 6.6 percent.

$$q_{m-10} = (0.326 \pm 0.004) \times 0.066 = 2.2 \times 10^{-2} \text{ mgmole/sec}$$

$$q_{m-20} = 4.3 \times 10^{-2} \text{ mgmole/sec}$$

$$t_{10} = (7.6+0.2) \times 10^{-2} \text{ mgmole} \times \frac{1 \text{ sec}}{2.2 \times 10^{-2} \text{ mgmole}}$$

$$= \underline{3.5 \pm 0.1 \text{ sec}}$$

$$t_{20} = \underline{1.8 \text{ sec}}$$

Development of Equation 7

From equation 5

$$k_g = \frac{1.82}{M} (\mu)^{0.51} \left[\frac{\rho_b D_v}{\mu}\right]^{2/3} \frac{G^{0.49}}{D_p^{0.51}}$$

The molecular diffusivity can be shown (Smith, 1956, p. 273) to be 0.083 cm^2/sec for a temperature of 76.2°F and a pressure of 653 mm Hg.

$$k_g = \frac{1.82}{43} (83 \times 10^{-6})^{0.51} \times \left[\frac{1.52 \times 10^{-3} \text{ g/cc} \times 83 \times 10^{-3} \text{ cm}^2/\text{sec}}{83 \times 10^{-6} \text{ g/cm-sec}}\right]^{2/3} \frac{G^{0.49}}{D_p^{0.51}}$$

$$k_g (\text{gmole/cm}^2\text{-sec}) = 4.9 \times 10^{-4} \, G^{0.49}/D_p^{0.51}$$

$$A(\text{cm})^2 = 6W/D_p \rho_s = \frac{6 \times 1.02 \text{ gm}}{D_p \text{cm} \times 0.7 \text{ g/cc}} = 8.7 D_p$$

$$kgA(\text{gmole/sec}) = 4.3 \times 10^{-3} \, G^{0.49}/D_p^{1.51}$$

$$kgA(\text{cc/sec}) = \frac{4.31 \times 10^{-3} \times 43 \text{ g/gmole}}{1.52 \times 10^{-3} \text{ g/cc}} \, G^{0.49}/D_p^{1.51}$$

$$k_gA(cc/sec) = 120\ G^{0.49}/D_p^{1.51}$$

$$R_f = 1/k_gA = \underline{0.0083\ D_p^{1.51}/G^{0.49}}$$

Development of Equation 9

$$R_s = \frac{(D_p/2)\lambda}{D_K(A/2)}$$

The Knudsen diffusivity (Smith, 1956, p. 268) equals 0.0051 cm^2/sec for a temperature of 76.2°F and for a pore radius of $2x10^{-7}$cm.

$$R_s(sec/cc) = \frac{(D_p/2)cm\lambda}{0.0051cm^2/sec \times \frac{8.7}{2D_p}\ cm^2}$$

$$= \underline{22\ \lambda\ D_p^2}$$

Development of Equation 11

From equations 4 and 10

$$R_i = \frac{L}{D_iA''} = \frac{L\rho_bC}{A''D_pG}\left[1 + 19.4(D_p/D_t)^2\right]$$

The area, A", for interstitial diffusion equals the vessel area multiplied by an assumed void fraction of 0.40

$$A'' = 3.10\ cm^2 \times 0.40 = 1.25\ cm^2$$

$$R_i = \frac{Lcm \times 1.52x10^{-3}g/cc \times C}{1.25\ cm^2 \times D_pcm \times Gg/cm^2\text{-sec}}\left[\frac{1 + 19.4D_p^2}{(1.98)^2}\right]$$

$$R_i(\text{sec/cc}) = 0.001LC \left[\frac{1.22 + 6.02\ D_p^2}{D_pG}\right]$$

The following table shows the values for C from Fahien and Smith (1955, p. 35):

D_p cm	Re_p	C
0.0975	5.4	-
0.184	10.2	5
0.278	15.4	7
0.390	21.6	8
0.585	32.4	9
0.0975	10.8	6
0.585	64.8	9

Table 5: Values for C in equation 11

APPENDIX II

Photograph 1: Complete composition-wave generator

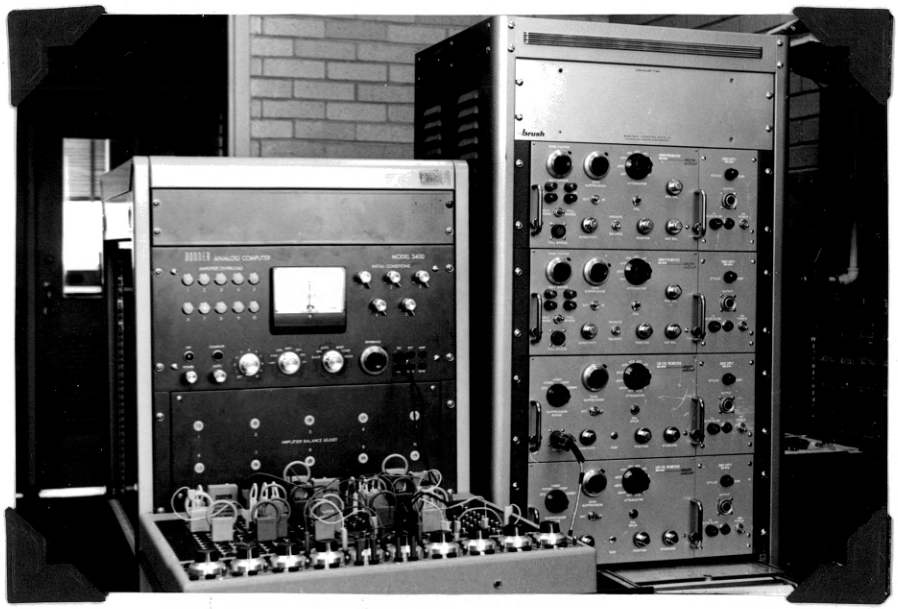

Photograph 2: Computor and recording system

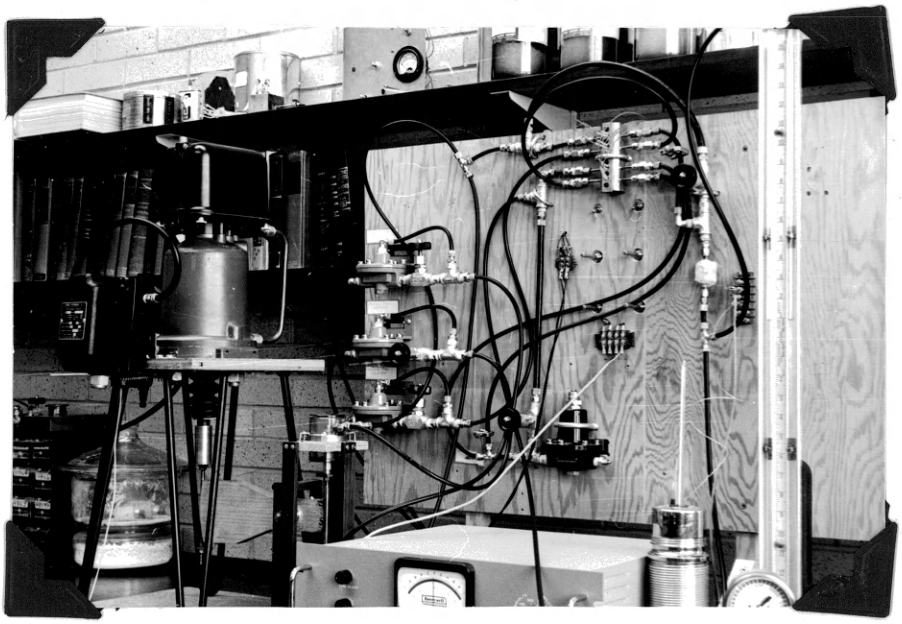

Photograph 3: Overall flow system

Table 6: Experimental run no. 12

Bed Size- Sand: Flow Rate- 10.0 cc/sec: Mean Bed Temp- $76.8 \pm 0.7^{o}F$: Bed Pressure- 9.7 in. H_2O: Atmospheric Temp and Pressure- $80.0^{o}F$ and 24.49 in. Hg: Input Composition Amplitude- $\pm 3.3\%$.

Frequency (cpm)	Amplitude Ratio	Phase Shift (degrees)
0.2	1.0	$-(12 \pm 2.4)$
0.3	1.0	$-(20 \pm 2)$
0.4	1.0	$-(24 \pm 4)$
0.5	1.0	- 30
0.6	0.99	- 36
0.8	0.99	- 48
1.0	0.97	- 60
1.5	0.90	- 90
1.75	0.87	-105
2.0	0.83	-120
2.5	0.80	-150
3.0	0.78	-180
3.5	0.74	-210
4.0	0.74	-252
4.5	0.75	-270
5.0	0.76	-300
6.0	0.76	-360
7.0	0.75	-420

Table 6, Continued

Frequency	Amplitude Ratio	Phase Shift
8.0	0.76	- 480
9.0	0.80	- 540
10	0.78	- 588
12.5	0.57	- 735
15	0.51	- 872
17.5	0.38 ± 0.01	-1030
20	0.49	-1176
25	0.27 ± 0.02	-1470
27.5	0.095 ± 0.015	-1615
30	0.32 ± 0.05	-1765

Table 7: Experimental run no. 13

Bed Size- 14/20-mesh: Flow Rate- 10.0 cc/sec: Mean Bed Temp- 76.5±0.3°F: Bed Pressure- 9.7 in. H_2O: Atmospheric Temp and Pressure- 79.2°F and 24.35 in. Hg: Input Composition Amplitude- ±3.3%: Maximum Temp Deviation- ±(0.50±0.01)°F

Frequency (cpm)	Amplitude Ratio		Phase Shift (degrees)	
	Composition	Temperature	Composition	Temperature
0.2	1.0	0.79	-7 and +12*	+28
0.3	0.98	0.90	-(3.6±1.8)	+17
0.4	0.98	0.98	-(4.8±2.4)	+3.7
0.5	0.96	1.0	-(6.0±3.0)	-4.5
0.6	0.89±0.01	1.0	-(7.2±3.6)	-5.4
0.7	0.85±0.02	0.94	-(8.4±4.2)	-6.3
0.8	0.79	0.91	-(9.6±4.8)	-12
0.9	0.74	0.88	-(10.4±5.4)	-20
1.0	0.72	0.89	-12	-21
1.25	0.63	0.82	-15	-26
1.5	0.53	0.78	-18	-40
1.75	0.40	0.72	-21	-48
2.0	0.28±0.01	0.64±0.01	-36	-51±3
2.1	0.26		-38	
2.2	0.24		-46	
2.3	0.23±0.01		-48	
2.4	0.29		-58	

*Propane lags and propylene leads.

Table 7, Continued

Frequency	Amplitude Ratio		Phase Shift	
	Composition	Temperature	Composition	Temperature
2.5	0.29	0.57	- 75	- 67
2.6	0.33		- 78	
2.7	0.35		- 97	
2.8	0.39		-101	
3.0	0.48	0.54 ± 0.01	$-(104 \pm 4)$	- 63
3.2	0.54 ± 0.01		- 96	
3.5	0.67	0.47 ± 0.02	-105	- 74
4.0	0.84	0.47 ± 0.02	-108	- 84
4.5	1.0	0.44 ± 0.01	- 81	- 95
5.0	1.1	0.46 ± 0.02	- 60	- 90
5.5	1.2	0.45	- 50	- 83
6.0	1.1	0.42	- 36	- 90
6.5	1.0	0.41	- 16	- 98
7.0	0.93	0.41 ± 0.02	0	$-(95 \pm 12)$
7.5	0.78	0.38	+ 11	- 92
8.0	0.60	0.39	+ 24	$-(87 \pm 10)$
8.5	0.39	0.38	+ 51	-103
9.0	0.24	0.40	+ 86	-105
9.25	0.21		+133	
9.5	0.26		+171	
9.75	0.34		+176	

Table 7, Continued

Frequency	Amplitude Ratio		Phase Shift	
	Composition	Temperature	Composition	Temperature
10	0.45	0.39	-156	- 94
11	0.79		-119	
12	1.2		- 87	
12.5		0.37		-117
13	2.1		- 47	
14	1.4		- 17	
15	1.0	0.38 ± 0.01	+ 18	-155
16	0.96 ± 0.03		+ 77	
16.5	0.86 ± 0.02		+139	
17	1.0		+163	
17.5	1.3 ± 0.1	0.37 ± 0.01	-168	-168
18	1.5 ± 0.2		-130	
19	2.4		- 91	
20	1.8	0.34 ± 0.02	- 48	$-(182 \pm 12)$
21	1.7 ± 0.2		- 25	
22	1.0 ± 0.05		$+(40 \pm 14)$	
23	0.97 ± 0.05		-276	
24	1.2 ± 0.1		-230	
25	1.5 ± 0.1	0.29 ± 0.04	$-(150 \pm 30)$	$-(232 \pm 15)$
26	1.9 ± 0.1		-125	
27	2.3 ± 0.1		- 97	

Table 7, Continued

Frequency	Amplitude Ratio		Phase Shift	
	Composition	Temperature	Composition	Temperature
28	2.4 ± 0.2		- 67	
29	1.2 ± 0.2		$-(35 \pm 25)$	
30	1.1 ± 0.2	0.25 ± 0.03	+ 36	$-(267 \pm 15)$

Table 8: Experimental run no. 15

Bed Size- 6/8-mesh: Flow Rate 10.0 cc/sec: Mean Bed Temp- $75.3 \pm 1.5^{o}F$: Bed Pressure- 10.1 in. H_2O: Atmospheric Temp and Pressure- $78.5 \pm 1.5^{o}F$ and 24.14 in. Hg: Input Composition Amplitude- +3.3%: Maximum Temp Deviation $\pm(0.26 \pm 0.02)^{o}F$.

Frequency (cpm)	Amplitude Ratio		Phase Shift (degrees)	
	Composition	Temperature	Composition	Temperature
0.2	1.0	1.0		+ 4.2
0.3	1.0	1.0	$-(3.6 \pm 1.8)$	$-(10 \pm 4)$
0.4	1.0	0.94	$-(4.8 \pm 2.4)$	- 22
0.5	0.97 ± 0.02	0.87	$-(6.0 \pm 3.0)$	$-(31 \pm 3)$
0.6	0.95	0.79	$-(7.2 \pm 3.6)$	- 41
0.7	0.92 ± 0.02	0.78	$-(8.4 \pm 4.2)$	- 40
0.8	0.86	0.73	$-(9.6 \pm 4.8)$	$-(50 \pm 5)$
0.9	0.85 ± 0.01	0.64	$-(10.6 \pm 5.3)$	$-(56 \pm 5)$
1.0	0.85 ± 0.01	0.59	$-(12 \pm 6)$	- 56
1.25	0.82 ± 0.02	0.53 ± 0.01	$-(11 \pm 4)$	- 70
1.5	0.73	0.48	- 18	- 67
1.75	0.68	0.40	- 21	- 78
2.0	0.59	0.37	- 24	$-(71 \pm 6)$
2.25	0.54 ± 0.01	0.33 ± 0.01	- 41	$-(80 \pm 7)$
2.5	0.54	0.33 ± 0.01	- 60	- 82
2.75	0.56 ± 0.01	0.29 ± 0.01	- 66	- 91
3.0	0.58	0.27 ± 0.01	- 72	- 99

Table 8, Continued

Frequency	Amplitude Ratio		Phase Shift	
	Composition	Temperature	Composition	Temperature
3.5	0.74 ± 0.01	0.22 ± 0.02	- 84	$-(95 \pm 20)$
4.0	0.94 ± 0.01	0.18 ± 0.02	- 96	$-(108 \pm 24)$
4.5	1.0	0.18 ± 0.04	- 81	$-(122 \pm 26)$
5.0	1.1	0.18 ± 0.02	- 75	$-(135 \pm 15)$
5.5	1.0	0.13 ± 0.02	- 66	$-(140 \pm 10)$
6.0	0.97	0.15 ± 0.03	- 54	-126
6.5	0.87	0.14 ± 0.01	- 58	-137
7.0	0.76	0.13 ± 0.01	- 42	$-(127 \pm 20)$
7.5	0.59		- 22	
8.0	0.41	0.12 ± 0.02	- 24	$-(145 \pm 25)$
8.5	0.19 ± 0.01		- 25	
9.0	0.083		-108	
9.5	0.25		-144	
10	0.42	0.12 ± 0.02	-132	$-(150 \pm 10)$
11	0.71		-119	
12	0.98		-101	
12.5	1.1	0.094 ± 0.011	- 90	$-(180 \pm 15)$
13	1.1		- 93	
13.5	0.98 ± 0.01		- 65	
14	0.74		- 50	
15	0.45		0	

Table 8, Continued

Frequency	Amplitude Ratio		Phase Shift	
	Composition	Temperature	Composition	Temperature
16	0.63 ± 0.01		-250	
16.5	1.1		-238	
17	1.5 ± 0.1		-204	
18	2.2 ± 0.1		-173	
19	1.9 ± 0.1		-137	
20	1.5		-120	
21	1.0 ± 0.1		- 76	
22	0.81 ± 0.03		- 26	
23	0.92 ± 0.03		-332	
24	1.2		-288	
25	1.4 ± 0.1		-240	
26	1.4		-218	
27	1.5 ± 0.1		$-(146 \pm 16)$	
28	1.7 ± 0.1		-100	
29	0.77 ± 0.06		- 35	
30	0.44 ± 0.10		0	

Table 9: Experimental run no. 14

Bed Size- 3/4-mesh: Flow Rate- 10.0 cc/sec: Mean Bed Temp- 77.5°F: Bed Pressure- 9.6 in. H_2O: Atmospheric Temp and Pressure- 80.8°F and 24.66 in. Hg: Input Composition Amplitude- +3.3%.

Frequency (cpm)	Amplitude Ratio	Phase Shift (degrees)
0.2	1.0	-12 and +14*
0.3	1.0	-3.6 and +7.2*
0.4	1.1	$-(4.8\pm2.4)$
0.5	0.96 ± 0.03	$-(6.0\pm3.0)$
0.6	1.0	$-(7.2\pm3.6)$
0.7	1.0	$-(8.4\pm4.2)$
0.8	0.94 ± 0.03	$-(9.6\pm4.8)$
0.9	0.94 ± 0.01	$-(11\pm5.4)$
1.0	0.91	$-(12\pm6.0)$
1.25	0.90 ± 0.01	$-(15\pm7.5)$
1.5	0.86	- 18
1.75	0.81	- 21
2.0	0.76	- 24
2.25	0.73	- 27
2.5	0.65	- 30
2.75	0.67	- 33
3.0	0.66	- 54
3.5	0.70	- 63

* Propane lags and propylene leads

Table 9, Continued

Frequency	Amplitude Ratio	Phase Shift
4.0	0.74	- 72
4.5	0.83	- 81
5.0	0.84	$-(83\pm7)$
5.5	0.84	$-(74\pm9)$
6.0	0.84	- 72
6.5	0.83	- 59
7.0	0.79	- 42
7.5	0.67	- 45
8.0	0.60 ± 0.02	- 48
8.5	0.49	- 51
9.0	0.41 ± 0.02	- 54
9.5	0.29	- 86
10	0.28 ± 0.01	$-(96\pm12)$
10.5	0.33	-114
11	0.40 ± 0.03	$-(116\pm6)$
12	0.68	-115
13	0.68 ± 0.01	$-(94\pm7)$
14	0.63	-101
15	0.45	- 90
16	0.24 ± 0.02	- 77
16.5	0.12 ± 0.02	$-(139\pm19)$

Table 9, Continued

Frequency	Amplitude Ratio	Phase Shift
17	0.26 ± 0.02	-184
18	0.50 ± 0.01	-194
19	0.61 ± 0.01	$-(148 \pm 12)$
20	0.51 ± 0.01	-144
21	0.43 ± 0.02	-151
22	0.33 ± 0.02	-105
23	0.15 ± 0.02	$-(110 \pm 28)$
24	zero	
25	0.21 ± 0.04	$-(240 \pm 30)$
26	0.32 ± 0.03	$-(218 \pm 32)$
27	0.50 ± 0.03	$-(194 \pm 15)$
28	0.75 ± 0.04	$-(185 \pm 20)$
29	0.14 ± 0.05	$-(139 \pm 35)$
30	zero	

Table 10: Experimental run no. 19

Bed Size- Sand: Flow Rate- 20.0 cc/sec: Mean Bed Temp- $79.5 \pm 1.0^{o}F$: Bed Pressure- 1.85 in. Hg: Atmospheric Temp and Pressure- $80.8 \pm 1.0^{o}F$ and 24.42 in. Hg: Input Composition Amplitude- $\pm 3.3\%$.

Frequency (cpm)	Amplitude Ratio	Phase Shift (degrees)
0.4	1.0	$-(12 \pm 2)$
0.5	1.0	$-(15 \pm 3)$
0.6	1.0	$-(18 \pm 4)$
0.7	1.0	$-(21 \pm 4)$
0.8	1.0	$-(24 \pm 4)$
0.9	0.98	$-(27 \pm 5)$
1.0	0.96	$-(33 \pm 3)$
1.25	0.91	$-(41 \pm 3)$
1.5	0.89	$-(50 \pm 4)$
1.75	0.87	$-(58 \pm 5)$
2.0	0.84 ± 0.02	$-(66 \pm 6)$
2.25	0.81	$-(74 \pm 6)$
2.5	0.75	$-(82 \pm 7)$
2.75	0.76	$-(91 \pm 8)$
3.0	0.74	$-(99 \pm 9)$
3.5	0.75	$-(115 \pm 10)$
4.0	0.76	$-(132 \pm 12)$
4.5	0.76	$-(148 \pm 14)$

Table 10, Continued

Frequency	Amplitude Ratio	Phase Shift
5.0	0.78	-165
5.5	0.82	-182
6.0	0.81	-198
6.5	0.84	-214
7.0	0.81	-231
7.5	0.78	-248
8.0	0.68 ± 0.01	-264
8.5	0.68 ± 0.02	-280
9.0	0.68 ± 0.01	-296
9.5	0.68	-313
10	0.67	-324
11	0.70	$-(356 \pm 13)$
12	0.73	-390
13	0.70	-422
14	0.63 ± 0.02	-454
15	0.60 ± 0.02	-468
16	0.56	-518
17	0.50 ± 0.03	-550
18	0.46 ± 0.02	-583
19	0.38 ± 0.02	-615
20	0.36 ± 0.01	-648
21	0.38 ± 0.02	-680

Table 10, Continued

Frequency	Amplitude Ratio	Phase Shift
22	0.33 ± 0.01	-713
23	0.30 ± 0.01	-745
24	0.30 ± 0.01	-778
25	0.31 ± 0.03	-810
26	0.32 ± 0.04	-842
27	0.31 ± 0.01	-875
28	0.31 ± 0.01	-907
29	0.32 ± 0.02	-940
30	0.32 ± 0.02	-972

Table 11: Experimental run no. 18

Bed Size- 14/20-mesh: Flow Rate 20.0 cc/sec: Mean Bed Temp- 73.7±3.3°F: Bed Pressure- 1.90 in. Hg: Atmospheric Temp and Pressure- 77.2±2.7°F and 24.49 in. Hg: Input Composition Amplitude- ±3.3%: Maximum Temp Deviation- ±(0.58±0.04)°F.

Frequency (cpm)	Amplitude Ratio		Phase Shift (degrees)	
	Composition	Temperature	Composition	Temperature
0.4	1.0	0.83	-(3.6±2.4)	+(16±2)
0.5	1.0	0.96	-(4.5±3.0)	+10
0.6	1.0	0.98±0.01	-(5.4±3.6)	+ 5
0.7	0.99±0.02	1.0	-(6.3±4.2)	- 2
0.8	1.0	1.0	-(7.2±4.8)	- 3
0.9	1.0	1.0	-(8.1±5.4)	- 8
1.0	1.0	1.0	-(9.0±6.0)	-15
1.25	1.0	1.0	-(11±7.5)	-18
1.5	0.96	1.0	-(14±9.0)	-22
1.75	0.87±0.02	0.92	-(16±10)	-(26±10)
2.0	0.80	0.96±0.04	-(18±12)	-30
2.25	0.73±0.01	0.88±0.04	-(20±14)	-36
2.5	0.68±0.02	0.81±0.04	-(23±15)	-37
2.7	0.57±0.03	0.84	-(25±17)	-41
3.0	0.47±0.02	0.76±0.03	-(27±18)	-44
3.5	0.38±0.01	0.72±0.05	-(53±21)	-(64±10)
4.0	0.46±0.01	0.72±0.05	-(84±24)	-60

Table 11, Continued

Frequency	Amplitude Ratio		Phase Shift	
	Composition	Temperature	Composition	Temperature
4.5	0.57 ± 0.01	0.64	$-(95 \pm 14)$	- 68
5.0	0.64 ± 0.02	0.56	$-(105 \pm 15)$	- 75
5.5	0.66 ± 0.02	0.48	-116	- 83
6.0	0.77	0.44 ± 0.02	$-(108 \pm 18)$	- 90
6.5	0.83 ± 0.01	0.41 ± 0.01	-117	- 78
7.0	0.85 ± 0.01	0.37 ± 0.02	$-(105 \pm 21)$	- 85
7.5	0.82 ± 0.03	0.34 ± 0.02	-112	- 91
8.0	0.87 ± 0.05	0.31	- 96	$-(85 \pm 12)$
8.5	0.78	0.27	- 77	- 78
9.0	0.79	0.25 ± 0.02	- 81	- 83
9.5	0.75 ± 0.03	0.23 ± 0.02	- 57	$-(74 \pm 15)$
10	0.73 ± 0.03	0.26 ± 0.01	- 36	$-(85 \pm 6)$
11	0.57 ± 0.03	0.24 ± 0.01	- 40	- 75
12	0.46 ± 0.01	0.20 ± 0.01	$-(29 \pm 14)$	- 83
13	0.27 ± 0.01	0.21 ± 0.02	$+(16 \pm 16)$	$-(83 \pm 8)$
14	0.23 ± 0.01	0.18 ± 0.01	$+(50 \pm 16)$	$-(73 \pm 8)$
15	0.22 ± 0.01	0.17 ± 0.01	$+(90 \pm 18)$	- 70
16	0.39 ± 0.01	0.19 ± 0.01	$+(125 \pm 20)$	- 56
17.5	0.56 ± 0.01	0.17 ± 0.01	$-(153 \pm 10)$	- 63
18	0.70 ± 0.01	0.15 ± 0.01	$-(119 \pm 10)$	- 65
19	0.81 ± 0.01	0.12 ± 0.04	- 91	$-(58 \pm 10)$

Table 11, Continued

Frequency	Amplitude Ratio		Phase Shift	
	Composition	Temperature	Composition	Temperature
20	0.89 ± 0.02	0.13 ± 0.02	- 48	- 50
21	0.92 ± 0.02	0.12 ± 0.02	- 25	- 53
23	0.87 ± 0.03	0.10 ± 0.01	$-(14 \pm 14)$	- 56
24	0.77 ± 0.04	0.10 ± 0.01	$+(14 \pm 14)$	- 64
25	0.61 ± 0.03	0.11 ± 0.01	+120	$-(52 \pm 15)$
26	0.65 ± 0.04	0.098 ± 0.01	-250	$-(55 \pm 15)$
27	0.71 ± 0.04	0.086 ± 0.01	-195	$-(58 \pm 15)$
29	0.71 ± 0.04	0.082 ± 0.01	-174	$-(66 \pm 17)$
30	0.65 ± 0.04	0.092 ± 0.01	-108	$-(70 \pm 18)$

Table 12: Experimental run no. 17

Bed Size- 3/4-mesh: Flow Rate 20.0 cc/sec: Mean Bed Temp- 78.5°F: Bed Pressure- 1.90 in. Hg: Atmospheric Temp and Pressure- 81.7°F and 24.22 in. Hg: Input Composition Amplitude- ±3.3%.

Frequency (cpm)	Amplitude Ratio	Phase Shift (degrees)
0.4	1.0	$-(2.4\pm2.4)$
0.5	1.0	$-(3.0\pm3.0)$
0.6	1.0	$-(3.6\pm3.6)$
0.7	1.0	$-(4.2\pm4.2)$
0.8	1.0	$-(4.8\pm4.8)$
0.9	1.0	$-(5.4\pm5.4)$
1.0	1.0	$-(6.0\pm3.0)$
1.25	0.97	$-(7.5\pm3.8)$
1.5	0.99	$-(9.0\pm4.5)$
1.75	0.90	$-(10\pm5.0)$
2.0	0.88	$-(12\pm6.0)$
2.25	0.87	$-(14\pm7.0)$
2.5	0.91 ± 0.02	$-(15\pm7.5)$
2.75	0.89	$-(17\pm8.5)$
3.0	0.87 ± 0.05	$-(18\pm9.0)$
3.5	0.91	$-(21\pm10)$
4.0	0.92	$-(24\pm12)$
4.5	0.92	$-(27\pm13)$
5.0	0.90	$-(30\pm15)$

Table 12, Continued

Frequency	Amplitude Ratio	Phase Shift
5.5	0.94	- 33
6.0	0.93	- 36
6.5	1.0	- 39
7.0	1.0 ± 0.03	- 42
7.5	1.1	- 45
8.0	1.3 ± 0.1	- 48
8.5	1.4	- 51
9.0	1.3	- 27
9.5	1.3	- 29
10	1.3	- 24
11	1.0	- 13
12	0.69 ± 0.03	0
13	0.45	0
14	0.38 ± 0.03	$-(8.4 \pm 8.4)$
15	0.37 ± 0.03	$-(27 \pm 9)$
16	0.55	- 37
17	0.82 ± 0.03	- 61
18	1.2 ± 0.1	- 65
19	1.3	- 46
20	1.4	- 48
21	1.2	- 25
22	1.1	- 26

Table 12, Continued

Frequency	Amplitude Ratio	Phase Shift
23	0.52 ± 0.03	$-(28 \pm 14)$
24	zero	
25	0.61 ± 0.04	-150
26	1.3 ± 0.1	-125
27	1.7	$-(113 \pm 17)$
28	2.3 ± 0.1	-108
29	2.3 ± 0.1	$-(87 \pm 15)$
30	2.2 ± 0.1	- 72

Table 13: Experimental run no. 9

Bed Size- 14/20-mesh: Flow Rate- 10.0 cc/sec: Mean Bed Temp- 75.6±0.5°F: Bed Pressure- 9.9 in. H_2O: Atmospheric Temp and Pressure- 78.4±0.4°F and 24.23 in. Hg: Input Composition Amplitude- ±3.8%: Maximum Temp Deviation- ±0.60°F.

Frequency (cpm)	Amplitude Ratio		Phase Shift (degrees)	
	Composition	Temperature	Composition	Temperature
0.2	1.0	0.80	-(2.4±2.4)	+(31±1)
0.3	1.0	0.95	-(3.6±1.8)	+ 17
0.4	0.96	1.0	-(4.8±2.4)	+ 13
0.5	0.90	1.0	-(6.0±3.0)	0
0.6	0.87	1.1	-(7.2±3.6)	- 5.4
0.7	0.82	0.95	-(8.4±4.2)	- 23
0.8	0.76	0.97	-(9.6±4.8)	- 27
0.9	0.78	1.0	-(11±5.4)	- 19
1.0	0.71	0.95	-(12±6.0)	- 21
1.25	0.64	0.83	-(15±7.5)	- 26
1.5	0.56	0.80	- 18	-(35±4)
1.75	0.44	0.77	-(21±10)	- 58
2.0	0.30	0.70	-(36±12)	- 42
2.5	0.33	0.63	-(75±15)	- 52
3.0	0.57	0.59	- 90	- 43
3.5	0.74	0.57	-105	- 74
4.0	0.95	0.59	- 96	- 72

Table 13, Continued

Frequency	Amplitude Ratio		Phase Shift	
	Composition	Temperature	Composition	Temperature
5.0	1.2	0.56	- 60	- 90
6.0	1.1	0.49	- 36	- 90
7.0	0.88	0.50	0	-106
8.0	0.59	0.48	+ 24	-120
9.0	0.21	0.49	+ 81	-110
10	0.51	0.44	-168	-127
12.5	1.7	0.38	- 90	-162
15	1.4	0.31	0	-196
17.5	1.5 ± 0.1	0.22	-213	-210
20	1.1	0.16	- 96	-266
25	0.70 ± 0.04	0.10	-150	-277
30	0.34 ± 0.04		0	

Table 14: Experimental run no. 11

Bed Size- 6/8-mesh: Flow Rate 10.0 cc/sec: Mean Bed Temp- 75.1°F: Bed Pressure- 9.7 in. H_2O: Atmospheric Temp and Pressure- 77.9°F and 24.50 in. Hg: Input Composition Amplitude- ±3.8%: Maximum Temp Deviation- ±(0.31±0.02)°F.

Frequency (cpm)	Amplitude Ratio		Phase Shift (degrees)	
	Composition	Temperature	Composition	Temperature
0.1	1.0	1.0	-(1.2±1.2)	
0.2	1.0	1.0	-(2.4±2.4)	- 0.6
0.25		1.0		-11
0.3	1.0	0.97	-(3.6±3.6)	-(15±2)
0.4	0.99	0.92±0.02	-(4.8±2.4)	-(28±9)
0.5	0.98±0.05	0.83	-(6.0±3.0)	-34
0.6	0.99	0.80	-(7.2±3.6)	-41
0.7	1.0	0.70±0.03	-(8.4±4.2)	-(44±4)
0.8	0.92±0.03	0.71±0.02	-(9.6±4.8)	-(51±5)
0.9	0.91	0.65	-(11±5.4)	-51
1.0	0.89	0.70±0.01	-(12±6.0)	-57
1.25	0.81	0.53	-(15±7.5)	-(64±7)
1.5	0.78±0.04	0.48±0.01	-18	- 67
1.75	0.72	0.39±0.01	-(21±10)	-(74±5)
2.0	0.66	0.38±0.01	-24	- 78
2.5	0.57±0.02	0.30±0.02	-30	-(90±7)
2.75	0.59		-50	

Table 14, Continued

Frequency	Amplitude Ratio		Phase Shift	
	Composition	Temperature	Composition	Temperature
3.0	0.65±0.01	0.25±0.01	- 54	-(90±9)
3.5	0.79	0.23±0.01	- 63	-(105±15)
4.0	0.92±0.02	0.22±0.01	- 60	-(96±12)
4.5	1.0	0.18±0.01	- 67	-(102±8)
5.0	1.2±0.1	0.17±0.02	- 45	-(90±15)
6.0	1.1	0.17±0.01	- 36	-108
7.0	0.97	0.16	- 21	-(116±10)
8.0	0.70	0.13	0	-120
8.5	0.55		- 25	
9.0	0.41	0.13	- 27	-137
9.5	0.34		- 57	
10	0.37	0.13	- 84	-150
12.5	1.4	0.13	- 90	-(162±15)
15	1.1	0.10±0.01	- 18	-(195±18)
17.5	1.1		-188	
20	1.0		- 94	
22	0.45		- 28	
24	0.42		-202	
25	0.56±0.04		-180	
26	0.59		-124	
27	0.45±0.02		- 40	

Table 14, Continued

Frequency	Amplitude Ratio		Phase Shift	
	Composition	Temperature	Composition	Temperature
27.5	0.71		- 85	
28	0.45±0.05		-152	
29	0.37±0.02		-137	
30	0.30±0.05		-145	

Table 15: Experimental run no. 10

Bed Size- 3/4-mesh: Flow Rate- 10.0 cc/sec: Mean Bed Temp- $75.1 \pm 1.0^{o}F$: Bed Pressure- 9.9 in. H_2O: Atmospheric Temp and Pressure- $77.9 \pm 0.9^{o}F$ and 24.40 in. Hg: Input Composition Amplitude- ± 3.8.

Frequency (cpm)	Amplitude Ratio	Phase Shift (degrees)
0.2	1.0	
0.3	1.0	$-(3.6 \pm 3.6)$
0.4	0.98	$-(4.8 \pm 4.8)$
0.5	0.98	$-(6.0 \pm 3.0)$
0.6	1.0	$-(7.2 \pm 7.2)$
0.7	1.0	$-(4.2 \pm 4.2)$
0.9	0.94	$-(5.4 \pm 5.4)$
1.0	0.97 ± 0.02	$-(6.0 \pm 6.0)$
1.25	0.91 ± 0.04	- 7.5
1.5	0.87 ± 0.04	- 9.0
1.75	0.88	- 11
2.0	0.83	- 12
2.2	0.74	$-(13 \pm 13)$
2.5	0.69 ± 0.02	$-(15 \pm 15)$
2.75	0.72	- 17
3.0	0.78 ± 0.04	- 36
3.5	0.92	- 42
4.0	0.95 ± 0.02	- 48
4.5	1.1	- 41

Table 15, Continued

Frequency	Amplitude Ratio	Phase Shift
5.0	1.1	-(45±15)
6.0	1.1	-(54±18)
7.0	0.97	- 42
8.0	0.78±0.04	- 24
9.0	0.64	- 27
10	0.55	- 48
11	0.64	- 78
12	0.97	- 86
12.5	1.2	- 90
15	1.1	- 18
17.5	0.68±0.01	-190
20	1.0	-(84±12)
22	0.52±0.02	- 26
24	0.39±0.02	-173
25	0.54±0.02	-(165±15)
26	0.59±0.03	- 94
27.5	0.21±0.02	-(165±65)
30	0.30±0.05	-(72±18)

Table 16: Experimental run no. 7

Bed Size- 8/12-mesh: Flow Rate- 10.0 cc/sec: Mean Bed Temp- 76.9±0.6°F: Bed Pressure- 10.0 in. H_2O: Atmospheric Pressure- 24.28 in. Hg: Input Composition Amplitude- ±3.8%: Maximum Temp Deviation- ±(0.33±0.02)°F.

Frequency (cpm)	Amplitude Ratio		Phase Shift (degrees)	
	Composition	Temperature	Composition	Temperature
0.2	1.0	1.0	-(2.4±2.4)	- 9.0
0.5	1.0	0.61±0.03	-(6.0±3.0)	-(40±6)
1.0	0.88	0.48±0.01	-(6.0±6.0)	-(69±12)
2.0	0.57	0.31±0.01	-(12±12)	- 90
3.0	0.60	0.14±0.02	- 54	-(100±8)
4.0	0.99		- 72	
5.0	1.2		- 30	
6.0	1.1		0	
8.0	0.50		+ 24	
10	0.36		-(72±12)	
15	1.3		+ 62	
20	2.9		0	
30	0			

Table 17: Experimental run no. 4

Bed Size- 4/6-mesh: Flow Rate- 10.2 cc/sec: Mean Bed Temp- 71.6°F: Bed Pressure- 10.8 in. H_2O: Input Composition Amplitude- ±4.4%: Maximum Temp Deviation- ±0.52°F.

Frequency (cpm)	Amplitude Ratio		Phase Shift (degrees)	
	Composition	Temperature	Composition	Temperature
0.2	1.0		-(2.4±2.4)	
0.5	1.0	1.0	-(6.0±3.0)	-(25±3)
1.0	0.91	0.72	-(12±6)	-(33±12)
2.0	0.80±0.01	0.37±0.04	0	-(30±12)
5.0	1.1	0.19	- 30	-(57±12)
8.0	0.54±0.01	0.20	0	- 52
10	0.40		0	
20	1.5		0	

Table 18: Amplitude ratio at first resonances and experimental R/R_i ratios

Low mass velocity (4.6 mg/cm^2-sec)

D_p(cm)	Amplitude ratio		R/R_i ratio	
	±3.3% Deviation	±3.8% Deviation	±3.3% Deviation	±3.8% Deviation
0.0975	0.23±0.01	0.24±0.01	0.30±0.02	0.32±0.02
0.184		0.48±0.03		0.92±0.13
0.279	0.54±0.01	0.57±0.02	1.2	1.3±0.1
0.390		0.74±0.03		2.8±0.5
0.585	0.66±0.01	0.69±0.02	1.9±0.1	2.2±0.2

High mass velocity (9.2 mg/cm^2-sec)

D_p(cm)	Amplitude ratio	R/R_i ratio
	±3.3% Deviation	±3.3% Deviation
0.0975	0.38±0.01	0.61±0.03
0.585	0.88±0.02	7.3±1.7